

# Measurement Techniques and Challenges of Wireless LC Resonant Sensors

Masud, Mehedi; Vazquez, Patricia; Rehman, Muhammad Riaz; Elahi, Adnan; Wijns, William; Shahzad, Atif

DOI:

[10.1109/ACCESS.2023.3309300](https://doi.org/10.1109/ACCESS.2023.3309300)

License:

Creative Commons: Attribution (CC BY)

## Document Version

Version created as part of publication process; publisher's layout; not normally made publicly available

## Citation for published version (Harvard):

Masud, M, Vazquez, P, Rehman, MR, Elahi, A, Wijns, W & Shahzad, A 2023, 'Measurement Techniques and Challenges of Wireless LC Resonant Sensors: A Review', *IEEE Access*.  
<https://doi.org/10.1109/ACCESS.2023.3309300>

[Link to publication on Research at Birmingham portal](#)

## General rights

Unless a licence is specified above, all rights (including copyright and moral rights) in this document are retained by the authors and/or the copyright holders. The express permission of the copyright holder must be obtained for any use of this material other than for purposes permitted by law.

- Users may freely distribute the URL that is used to identify this publication.
- Users may download and/or print one copy of the publication from the University of Birmingham research portal for the purpose of private study or non-commercial research.
- User may use extracts from the document in line with the concept of 'fair dealing' under the Copyright, Designs and Patents Act 1988 (?)
- Users may not further distribute the material nor use it for the purposes of commercial gain.

Where a licence is displayed above, please note the terms and conditions of the licence govern your use of this document.

When citing, please reference the published version.

## Take down policy

While the University of Birmingham exercises care and attention in making items available there are rare occasions when an item has been uploaded in error or has been deemed to be commercially or otherwise sensitive.

If you believe that this is the case for this document, please contact [UBIRA@lists.bham.ac.uk](mailto:UBIRA@lists.bham.ac.uk) providing details and we will remove access to the work immediately and investigate.

Date of publication xxxx 00, 0000, date of current version xxxx 00, 0000.

Digital Object Identifier 10.1109/ACCESS.2023.0322000

# Measurement Techniques and Challenges of Wireless LC Resonant Sensors: A Review

MEHEDI MASUD<sup>1</sup>, PATRICIA VAZQUEZ<sup>1</sup>, MUHAMMAD RIAZ REHMAN<sup>1</sup>, ADNAN ELAHI<sup>2</sup>, WILLIAM WIJNS<sup>1</sup>, and ATIF SHAHZAD<sup>1,3</sup>

<sup>1</sup>Smart Sensors Laboratory, The Lambe Institute for Translational Medicine and Curam, College of Medicine, Nursing and Health Sciences, University of Galway, H91 TK33, Galway, Ireland

<sup>2</sup>Electrical and Electronic Engineering, School of Engineering, University of Galway, H91 TK33, Galway, Ireland

<sup>3</sup>Centre for Systems Modelling and Quantitative Biomedicine (SMQB), University of Birmingham, B15 2TT, United Kingdom

Corresponding author: William Wijns (e-mail: william.wyns@universityofgalway.ie).

This work was supported in part by the Department of Enterprise, Trade and Employment and Enterprise Ireland Disruptive Technology Innovation Fund under Grant DT20200210A, in part by the Science Foundation Ireland Research Professorship under Grant 15/RP/2765, and in part by University of Birmingham Dynamic Investment Fund.

## ABSTRACT

Wireless operation of the *LC* resonant sensor is based on magnetic coupling between two inductive coils, where the inductor of the sensor acts as a secondary coil for the magnetic coupling. An external reader coil is used as a primary coil to interrogate the sensor to detect the sensor's response. The wireless *LC* resonant sensor is applied in many applications where the cable connections for powering sensors and acquiring data are inconvenient. This review focuses on the fundamental operating principles of wireless *LC* resonant sensors, their measurement techniques, the challenges of accurately measuring the *LC* sensors, and their potential solutions. The main challenge in wireless measurement of the *LC* resonant sensor is to accurately measure the resonant frequency and the quality factor of the sensor which are solely dependent on the intrinsic parameters of the sensors. For practical wireless applications, it is crucial to interrogate *LC* resonant sensors regardless of their wireless measurement distances. To interrogate wireless *LC* resonant sensors, frequency and time domain measurements are commonly used. The coupling coefficient, which is greatly influenced by the geometrical dimensions and alignment of the two inductively coupled coils, has an adverse effect on distance independent readout in phase dip measurement in the frequency domain. Furthermore, the presence of parasitic capacitance that appears in parallel to the readout coil of the sensor has also an adverse effect on distance independent measurement in both frequency and time domain, resulting in an inaccurate measurement of the sensor's resonant frequency. A parasitic capacitance compensation technique can be employed to reduce or even eliminate the presence of parasitic capacitance in the readout coil, which significantly improves the measurement accuracy of the *LC* resonant sensor.

**INDEX TERMS** *LC*, wireless, Resonant sensor, Frequency domain, Time domain, Distance independent measurement

## I. INTRODUCTION

THE concept of wireless sensing gained significant attention after the introduction of "endo-radiosonde" in 1957, which is a smart capsule comprised of a transducer and radio transmitter that can be swallowed as a pill to monitor gastrointestinal pressure and wirelessly transmit the pressure value to the outside of the human body [1]. Collins published a pioneering work in 1967 on a miniaturised implantable 'transensor' based on a wireless resonant circuit for continuously monitoring intraocular pressure in rabbit eyes [2]. Subsequently, numerous studies were devoted to the design, fabrication, and experimental characterization of various or

other resonant sensor topologies to measure a variety of physical parameters, including pressure, temperature, humidity, biochemical species, gas, and more [3]–[10]. Wireless sensing of physical or biometric parameters of interest is advantageous for applications where cable connections are difficult or challenging to establish. In biomedical implants, for example, transcutaneous wires branching off the skin increase the risk of infection for short or long-term monitoring of the physiological parameters, compromising the patient's safety and comfort [11]. In practice, wireless sensors can be categorized into two groups: active sensors and passive sensors.

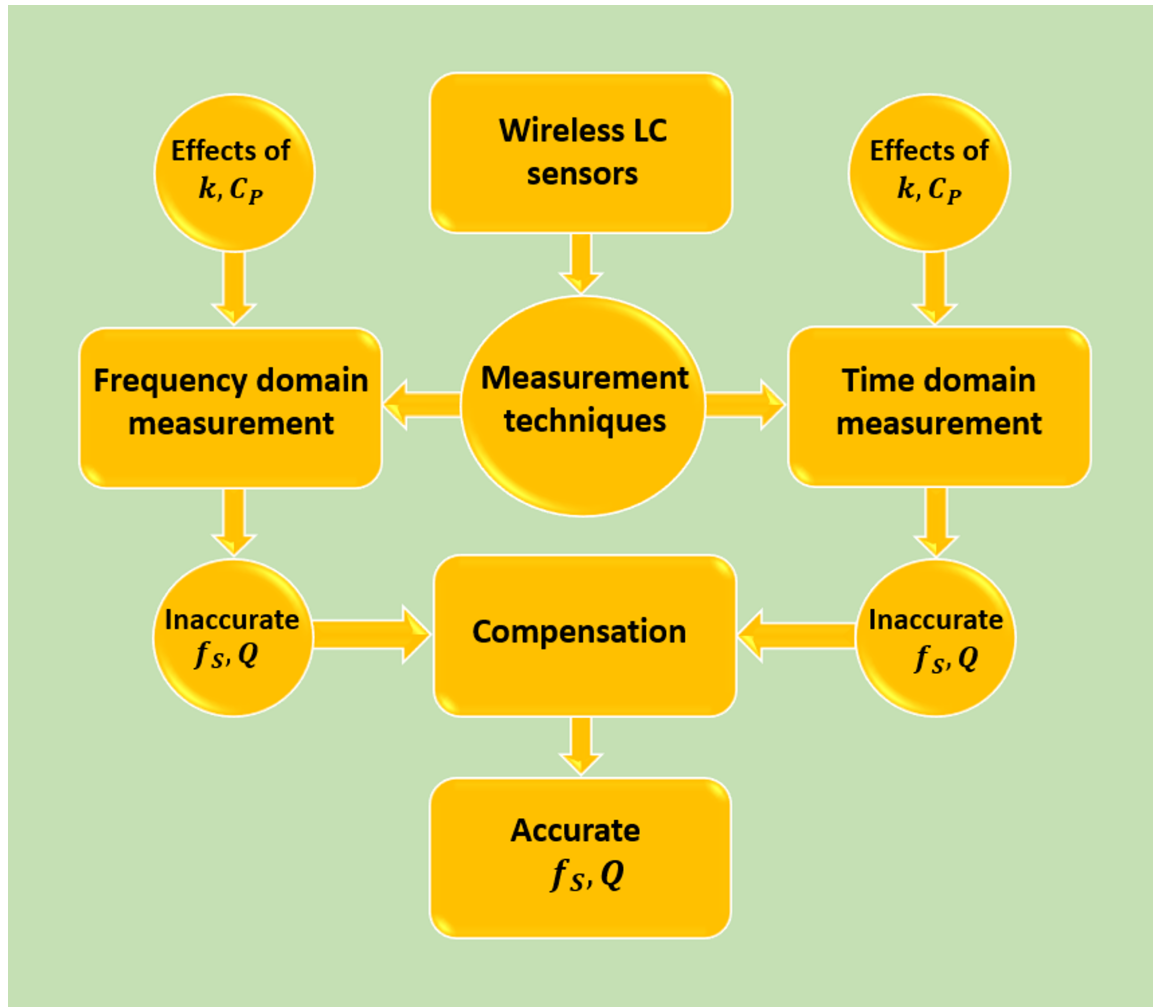


FIGURE 1. Block diagram representation of measurement techniques and challenges of wireless LC sensors.

Active sensors typically have signal processing and wide wireless data transmission capability, which complicates sensor configuration and necessitates active power supply, making them unsuitable for implants and applications in harsh environments [12]–[15]. Wireless passive sensors, on the other hand, are composed of passive elements—such as resistor, inductor, and capacitor—that only participate in data transmission and hence do not require an active power supply [16]–[19]. Passive sensors are therefore suitable for applications where cable connections are challenging, but their use necessitates a sophisticated reader system. Some active/semi-passive wireless sensors include batteries or energy harvesting capabilities: however, batteries must be replaced regularly, and low densities of scavenged energy and low conversion efficiency of the harvester make the passive operation of resonant sensors—such as LC—more appealing for wireless measurements [20]–[22]. For example, recent commercial success in wireless LC sensing technology is EndoSure Wireless AAA pressure sensor and ImPressure AAA Sac Pressure Sensor by CardioMems and Remon Medical Technologies [23], [24]. Endotronix, Inc.’s LC based pressure

sensor has also recently been investigated in human trials for Pulmonary Artery Pressure sensing with the Cordella Heart Failure System [25], [26].

Two measurement techniques, frequency and time domain, are widely applied to extract the resonance frequency and quality factor of a resonant sensor [27]. Frequency domain measurement is performed with either a bulky and expensive vector network analyser (VNA)/impedance analyser (IA) or custom designed front-end electronics with complex functionality to measure the reflection coefficients or the equivalent impedance of the sensors [28]–[33]. One of the frequency domain measurement techniques is phase dip which measures the phase of the equivalent impedance, and shows a dip in phase at resonant frequency of the sensors [34]–[36].

Despite having a wide dynamic range and better signal to noise ratio (SNR), the phase dip measurement technique is dependent on coupling coefficient, and requires a fixed wireless interrogation distance between the sensor and reader systems which is not suitable for wireless measurement of the sensors. Nopper et al. showed that instead of measuring the phase, the measurement of the real part of equivalent

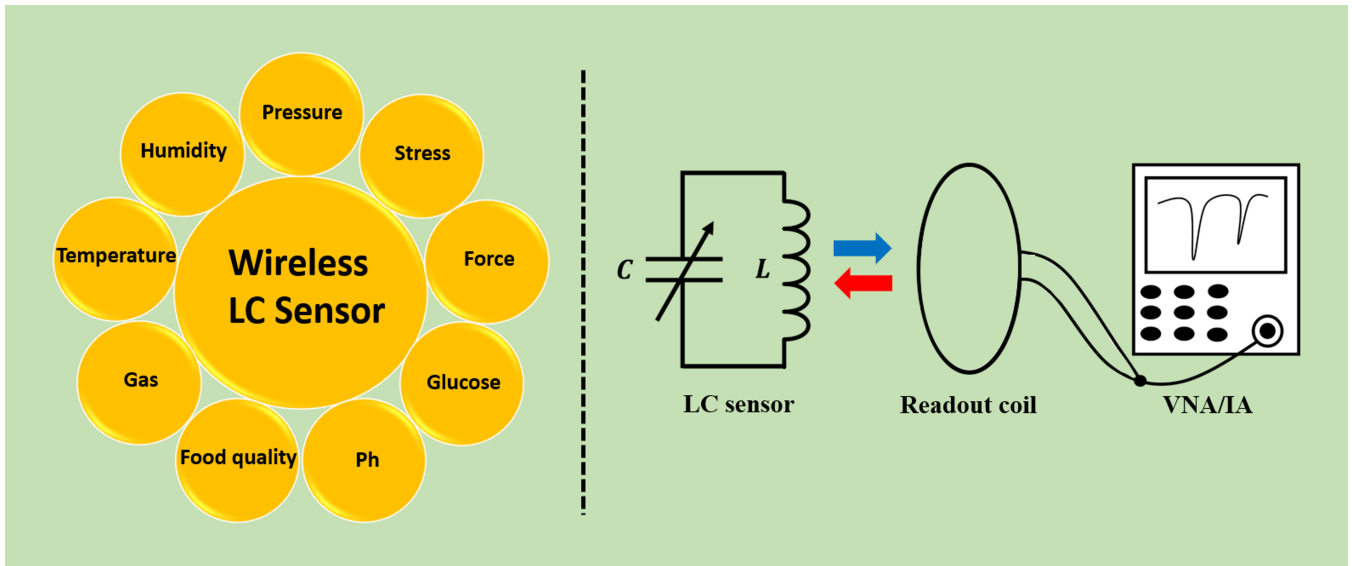


**FIGURE 2.** Typical schematic representation of the measurement of wireless  $LC$  resonant sensor by Vector Network Analyser (VNA)/ Impedance Analyser (IA) to measure different physical parameters.

impedance does not have a dependence on the  $k$  and hence, the wireless measurement distance [37], [38]. On the other hand, time domain measurement of the sensor utilises the damped decay response to extract the resonance frequency and quality factor of the sensors [39], [40]. Analytical modeling of the  $LC$  resonant sensors in the time domain shows that measurement of the resonant frequency is independent of the wireless interrogation distance. However, Demori et al. showed that measurement of the real part of equivalent impedance in the frequency domain and damped decay response in the time domain both suffer from undesired distance dependent measurement of  $LC$  sensors [65]. It is due to the fact that non avoidable parasitic capacitance appears in parallel to the readout coil of the sensors.

Although there has been significant progress in sensor design and applications, literature reporting the commonly practiced measurement techniques of the resonant sensors are sparse. Li et al. published a review on resonant sensors for harsh environmental applications which briefly covers the phase dip measurement techniques in the frequency domain [41]. Recently, Bhar et al. reported on the advancement of wireless  $LC$  sensors for temperature measurement which includes sensor design principles, sensor fabrication technologies, and materials [42]. Huang et al. covered a great deal of basic components of the sensors, sensing mechanisms, and measurement techniques both in time and frequency domain [43]. Not analyzed so far is the recent recognition of the effect of parasitic capacitance, which appears in parallel to the readout coil, resulting in inaccurate distance dependent measurement of the sensors in both time and frequency domain.

Therefore, this review covers the gap of recent developments on the measurement challenges of wireless  $LC$  resonant sensors by providing a comprehensive update on the

state-of-the-art and the background theory on the measurement techniques along with numerical simulations. Section (II) provides the background theory of the basic components of the sensors. Measurement techniques for both frequency and time domain are discussed in section (III) by providing analytical modeling, numerical simulation, and examples from experimental results. Wireless sensor measurement challenges are discussed in section (IV) by covering the effects on the presence of parasitic capacitance which appears in parallel to the readout coil, resulting distance dependent measurement of the sensors. Furthermore, section (V) covers the recently reported parasitic capacitance compensation technique which ceases the dependence of the parasitic capacitance for distance independent measurement of the sensor. Other sensor prospects and related discussions are covered in section (VI). The final section offers concluding remarks (VII). And a flowchart representing in Fig. 1 gives the gist of the paper.

## II. BASIC COMPONENTS OF LC SENSORS

An  $LC$  resonant sensor consists with basic electrical elements inductor  $L$  and capacitor  $C$ , where either of them can be used as a sensing element of the sensor. The majority of  $LC$  resonant sensors' sensing element is capacitive. The change of capacitance in response to the measurand of interest shifts the resonant frequency of the  $LC$  sensor. Much research is being conducted to improve the sensing capability of the sensing elements—capacitive sensor—in terms of performance, fabrication, and cost-effectiveness. As a result, new sensor designs and the search for new dielectric materials are unavoidable in order to address the unmet challenges.

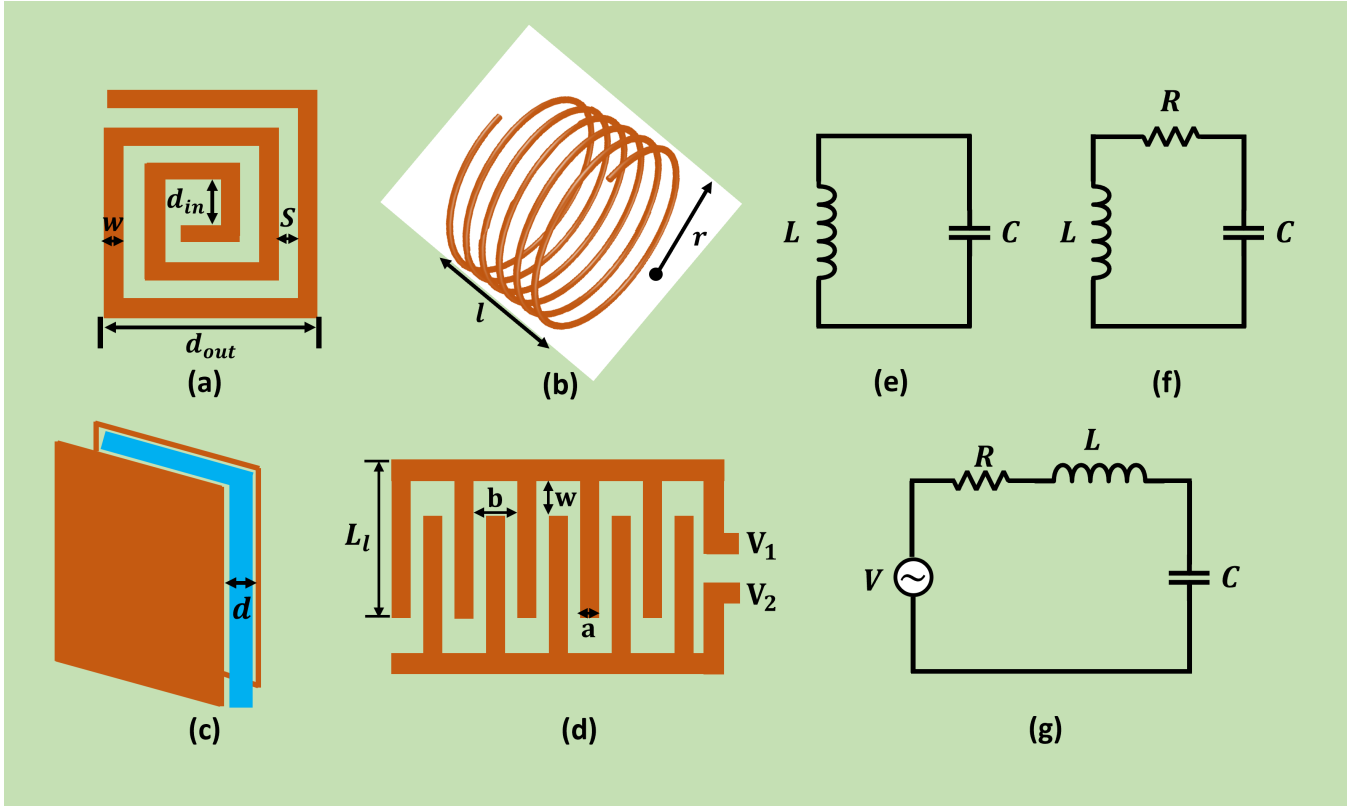


**FIGURE 3.** Schematic illustration of wireless LC resonant sensor components, (a) planar spiral inductor [49], (b) solenoid inductor, (c) parallel plate capacitor separated by distance  $d$ , (d) interdigitated capacitor [54], (e) LC resonant circuit, (f) RLC resonant circuit, (g) RLC resonant circuit with excitation source.

### A. INDUCTOR

To optimise the inductive coil for wireless interrogation of the LC sensors, various design topologies have been investigated. Sensor coils are typically designed using solenoid and planar spiral inductors. Fig. 3. (a) and 3. (b) show schematic representations of a planar square shape spiral inductor and a solenoid inductor coil, respectively. Despite having a lower quality factor, the inductance of the planar spiral inductor is well-defined over a wide range of process variations and widely used in electronics. Because of their simpler layout, square spiral inductors are more popular than hexagonal, octagonal, and circular inductors. Furthermore, apart from using the inductive coil for the purpose of electromagnetic coupling, it is also possible to make inductive coil as a sensing element of the sensors [44]–[47]. An inductive coil can be completely specified for a given shape as follows: number of turns  $n$ , turn width  $w$ , turn spacing  $s$ , outer diameter  $d_{out}$ , inner diameter  $d_{in}$ , average diameter  $d_{avg} = (d_{out} + d_{in}) / 2$  and fill ratio is defined as  $\rho = (d_{out} - d_{in}) / (d_{out} + d_{in})$  [48], [82]. For the discrete inductor, Wheeler developed several formulas for a planar spiral inductive coil. The inductance for a planar spiral inductor can be obtained using a straightforward modification of the original Wheeler formula as follows [49]:

$$L = K_1 \mu \frac{n^2 d_{avg}}{1 + K_2 \rho} \quad (1)$$

where  $\rho$  is the fill ratio,  $d_{avg}$  is the average diameter,  $\mu = \mu_0 \mu_r$  is the proportionality magnetic permeability, which is the product of the permeability of the free space  $\mu_0$ , and  $\mu_r$  is the permeability of the specific medium,  $K_1$  and  $K_2$  are layout dependent parameters with different values for square, hexagonal, and octagonal shapes. On the other hand, the inductance of the solenoid coil with a given length  $l$ , cross-sectional area  $A$ , and the number of turns  $N$  can be calculated by the basic physical law of electromagnetics as follows:

$$L = \frac{\mu N^2 A}{l} \quad (2)$$

### B. CAPACITOR

Capacitive sensors are commonly used as a sensing element of wireless LC resonant sensors for many applications [50]–[53]. Among various capacitive sensing topologies, parallel plate and interdigitated capacitors are widely implemented for practical applications, as shown in Fig. 3. (c), and 3. (d), respectively. A parallel plate capacitive sensor is typically designed by implementing the fundamental formula of the capacitance, which can be expressed as:

$$C = \frac{\epsilon_0 \epsilon_r A}{d} \quad (3)$$

where  $\epsilon_0 = 8.85 \times 10^{-12}$  F/m is the permittivity of free space,  $\epsilon_r$  is the relative permittivity of dielectric,  $A$  is the

surface area of the plates, and  $d$  is the separation gap between the two plates. On the other hand, the total capacitance of the interdigitated capacitor is calculated by the following formula [54]:

$$C_{\text{total}} = C_{uc}(N - 1)L_l \quad (4)$$

Where  $N$  is the number of unit cells of the capacitor,  $L_l$  is the length of the electrode fingers, and  $C_{uc}$  is the unit cell capacitance per length and can be written as:

$$C_{uc} = \varepsilon_0 (\varepsilon_r + \varepsilon_k) \frac{K_1 \left( \sqrt{1 - \left(\frac{a}{b}\right)^2} \right)}{K_1 \left(\frac{a}{b}\right)} + 2\varepsilon_0 \varepsilon_k \frac{t}{a} \quad (5)$$

where  $\varepsilon_0$  is the vacuum permittivity,  $\varepsilon_r$  is the dielectric constant of the substrate,  $\varepsilon_k$  is the dielectric constant of the dielectric film,  $K_1$  is the complete elliptic integral of the first kind,  $t$  is the electrode thickness,  $a$  is the electrode's width,  $b$  is the distance between fingers.

### C. LC RESONANT CIRCUIT

An  $LC$  resonant tank circuit, as shown in Fig. 3. (e), can be used to derive the electric equivalent  $LC$  resonant sensor. However, the internal structure of the  $LC$  sensor is basically an  $RLC$  circuit where the resistive component  $R$  appears from the equivalent series resistance of the inductive coil  $L$  and the capacitor  $C$ , and hence  $LC$  sensors are often referred to as  $RLC$  sensors as shown in Fig. 3. (f). The analytical expression for  $RLC$  resonant circuit under the excitation source shown in Fig. 3. (g) in Laplace domain for complex frequency  $s = j\omega$  can be derived as follows by applying Kirchhoff's Voltage Law (KVL) [55]:

$$V(S) = I(S) \left( sL + \frac{1}{sC} + R \right) \quad (6)$$

The impedance of the  $RLC$  circuit can be written as follows after rearranging equation (6):

$$Z(S) = \frac{V(S)}{I(S)} = sL + \frac{1}{sC} + R = \frac{s^2LC + sCR + 1}{sC} \quad (7)$$

Under the resonance condition, the energy supplied to the  $RLC$  resonant circuit will oscillate between the capacitor and the inductor, and the impedance  $Z(S)$  will be at its minimum. Therefore, the equation (7) can be expressed as follows by setting  $Z = 0$ :

$$s^2 + s\frac{R}{L} + \frac{1}{LC} = 0 \quad (8)$$

which is a quadratic equation and its roots are as follows:

$$s_{1,2} = -\frac{R}{2L} \pm \sqrt{\left(\frac{R}{2L}\right)^2 - \frac{1}{LC}} \quad (9)$$

The response the  $RLC$  circuit will be overdamped, critically damped, and underdamped, for  $\frac{R}{2L} > \frac{1}{\sqrt{LC}}$ ,  $\frac{R}{2L} = \frac{1}{\sqrt{LC}}$  and

$\frac{R}{2L} < \frac{1}{\sqrt{LC}}$ , respectively. When the equation (8) is underdamped condition, the roots become complex conjugate and can be written as:

$$s_{1,2} = -\frac{R}{2L} \pm j\sqrt{\frac{1}{LC} - \left(\frac{R}{2L}\right)^2} \quad (10)$$

where,  $\frac{R}{2L} = \alpha$ , damping constant  
 $\omega_0 = \frac{1}{\sqrt{LC}}$ , undamped natural resonant frequency  
 $\omega_d = \sqrt{\omega_0^2 - \alpha^2}$ , damped natural resonant frequency

The quantity  $\omega_0$  is the angular frequency of the oscillation when there is no resistive element is present in the circuit as Fig. 3. (e). On the other hand, the damped frequency  $\omega_d$  is always less than the undamped natural resonant frequency due to the presence of resistive element in the circuit as shown in Fig. 3. (f).

However, the  $RLC$  resonant circuit exhibits both a natural and forced response when an excitation source is used. Depending on how much resistive element is present in the circuit, the  $RLC$  circuit's natural response can be underdamped, critically damped, or overdamped. Since resistive components are present in every practical  $LC$  circuit, the response of the circuit will always be transient in nature and die out after a short period of time for natural response. On the other hand, the forced response is determined by the circuit's excitation source. The source continuously maintains the response in the circuit after the transient has passed and the circuit has reached steady state, which is known as steady state response [55]. These resonant principles are utilized in frequency and time domain measurement technique to measure wireless  $LC$  resonant sensor, as discussed in section (III).

Moreover, IA or VNA is often used to detect the resonant frequency of the sensors by monitoring the impedance of the readout coils or input return loss. These measuring instruments are expensive and bulky, and are only suitable for laboratory measurements. A few compact electronics systems were reported by several research groups which require less complex circuitry and less power budget to interrogate the wireless  $LC$  resonant sensors [56]–[59].

## III. MEASUREMENT TECHNIQUES OF LC SENSORS

Two types of measurement techniques, namely frequency-domain and time domain are commonly applied for wireless measurement of  $LC$  resonant sensors. Detailed analytical modelling and corresponding numerical simulations have been analysed and discussed for both measurement domains, highlighting their respective challenges.

### A. FREQUENCY DOMAIN MEASUREMENT

The equivalent circuit of the magnetic coupling passive  $LC$  resonant sensor is depicted in Fig. 4. (a). The circuit can be expressed analytically using the impedance transformer equations for harmonic oscillations with complex frequency  $f$ , and the induced voltage in the primary coil  $L_1$  and secondary coil  $L_2$  can be written in the Laplace domain as follows [59]:

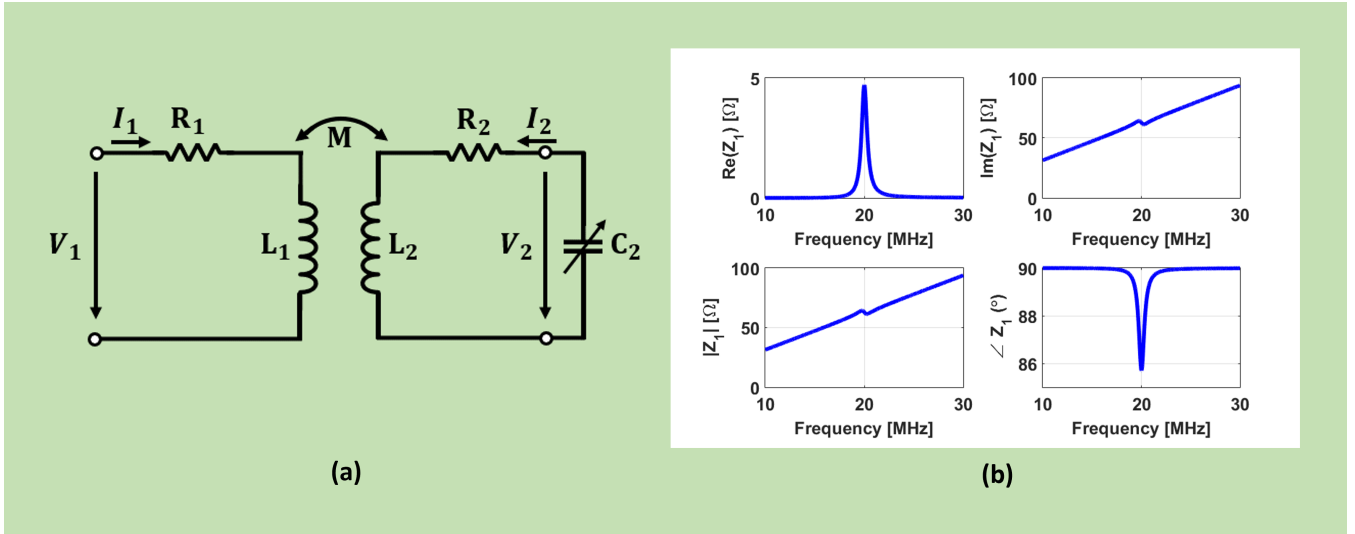


**FIGURE 4.** (a) Equivalent circuit of the inductively coupled LC sensor system [59]. (b) Numerical simulation of the equivalent impedance at the terminal of the readout coil with resonant frequency of the sensor  $f_s = 20\text{MHz}$ ,  $R_1 = 1\Omega$ ,  $L_1 = 0.5\mu\text{H}$ ,  $Q = 30$ , and  $k = 0.05$  [59].

$$V_1 = R_1 I_1 + sL_1 I_1 + sMI_2 \quad (11)$$

$$V_2 = R_2 I_2 + sL_2 I_2 + sMI_1 \quad (12)$$

where  $V_1$ ,  $V_2$ ,  $I_1$  and  $I_2$  are the voltage and current of the primary and secondary sides of the inductive coupling coils, respectively. The equivalent series resistance of the primary and secondary coils is represented by the circuit elements  $R_1$  and  $R_2$ , respectively. The parameter  $s$  is the complex frequency which can be written as  $s = j\omega = j2\pi f$ . The amount of inductive coupling between primary and secondary coil is measured by the mutual inductance  $M$  and can be written as:

$$M = k\sqrt{L_1 L_2} \quad (13)$$

where  $k$  is the geometry-dependent coupling coefficient of the mutual inductance  $M$ , which is dimensionless and ranges from 0 to  $\pm 1$ . Maximum coupling occurs when  $k = 1$ , and no coupling occurs when  $k = 0$ . The sensing element of the LC circuit—capacitive sensor,  $C_2$ —is connected to the secondary coil  $L_2$  of the inductive coupling, and the current flowing through the secondary part of the circuit can be written as:

$$I_2 = -sC_2 V_2 \quad (14)$$

The equivalent impedance  $Z_1$  at the primary side or the readout coil can be derived by combining the equations (11), (12), and (14), i.e.,

$$Z_1 = \frac{V_1}{I_1} = R_1 + j2\pi f L_1 + \frac{(2\pi f)^2 M^2}{R_2 + j\left(2\pi f L_2 - \frac{1}{2\pi f C_2}\right)} \quad (15)$$

The resonance frequency  $f_s$ , and quality factor  $Q$  of the LC sensor can be written as follows:

$$f_s = \frac{1}{2\pi\sqrt{L_2 C_2}}, \quad Q = \frac{1}{R_2} \sqrt{\frac{L_2}{C_2}} \quad (16)$$

By substituting equation (16) in (15), the equivalent impedance  $Z_1$  can be derived and separated between real and imaginary parts, i.e.,

$$Z_1 = R_1 + j2\pi f L_1 \left( 1 + \frac{k^2 \left(\frac{f}{f_s}\right)^2}{1 + j\frac{f}{Qf_s} - \left(\frac{f}{f_s}\right)^2} \right) \quad (17)$$

$$R_e \{Z_1\} = R_1 + 2\pi f L_1 k^2 Q \frac{\frac{f}{f_s}}{1 + Q^2 \left(\frac{f}{f_s} - \frac{f_s}{f}\right)^2} \quad (18)$$

$$I_m \{Z_1\} = 2\pi f L_1 \left( 1 + k^2 Q^2 \frac{1 - \left(\frac{f}{f_s}\right)^2}{1 + Q^2 \left(\frac{f}{f_s} - \frac{f_s}{f}\right)^2} \right) \quad (19)$$

The modulus of equivalent impedance  $|Z_1|$ , and phase angle  $\angle Z_1$  can be written as follows:

$$|Z_1| = \sqrt{R_e^2 \{Z_1\} + I_m^2 \{Z_1\}} \quad (20)$$

$$\angle Z_1 = \tan^{-1} \frac{I_m \{Z_1\}}{R_e \{Z_1\}} \quad (21)$$

Fig. 4. (b) illustrates the numerically simulated frequency response of the equivalent impedance for the equations of (18), (19), (20), and (21) by incorporating the sensor parameters of  $R_1 = 1\Omega$ ,  $L_1 = 0.5\mu\text{H}$ ,  $f_s = 20\text{MHz}$ ,  $Q = 30$ , and  $k = 0.05$ .

These derivations can be implemented in steady state or frequency domain measurement for wireless LC sensor. Phase dip and dip meter are two measurement methods that are frequently used in frequency domain analysis. The phase dip technique measures the equivalent impedance's phase angle, whereas the dip meter technique measures the maximum real part of the equivalent impedance  $Z_1$ .

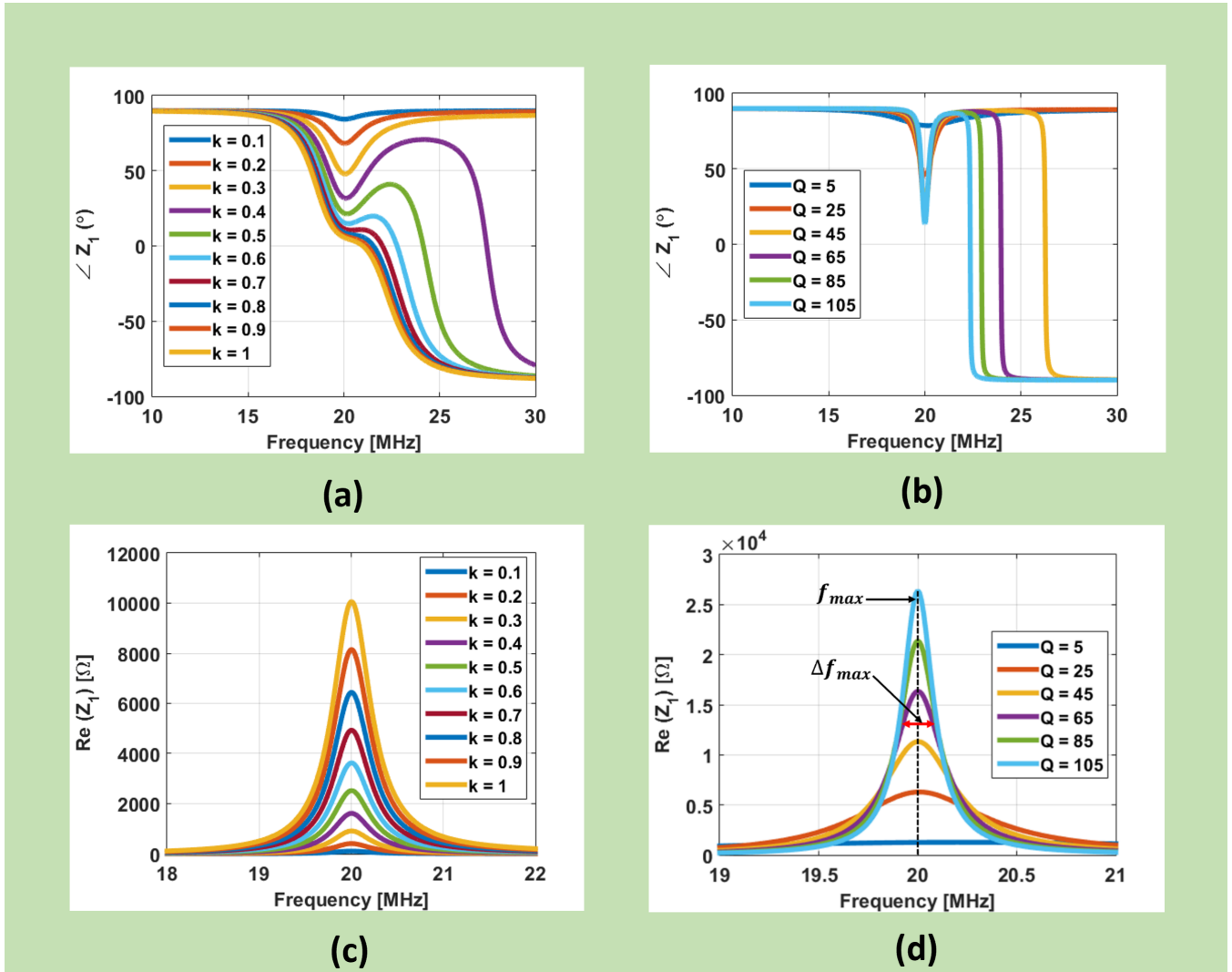


**FIGURE 5.** (a) Simulated equivalent impedance phase as a function of frequency for different values of coupling coefficient  $k$  [59], (b) the effect of different values of quality factor  $Q$  on the impedance phase, (c) maximum real part of the equivalent impedance as a function of frequency for different values of  $k$  [59], (d) the effect of different values of  $Q$  on the maximum real part of the equivalent impedance.

### 1) PHASE DIP MEASUREMENT IN FREQUENCY DOMAIN

An IA or VNA is usually employed to determine the resonant frequency of the  $LC$  sensor by measuring the phase angle  $\angle Z_1$  of the equivalent impedance in equation (21), and such measurement techniques have been reported in several publications [60], [61]. In phase dip measurement, the impedance phase minimum occurs at a frequency of  $f_{\phi, \min}$ . The derivative of the equation (21) can be set to zero with respect to frequency  $f$  to obtain the analytical expression of the phase minimum, which can be expressed as [59]:

$$\frac{\partial \angle Z_1}{\partial f} = 0 \quad (22)$$

which yields  $f_{\phi, \min}$  as:

$$f_{\phi, \min} \approx \left(1 + \frac{1}{4}k^2 + \frac{1}{8Q^2}\right) f_s \quad (23)$$

Equation (23) demonstrates that minimum phase of the equivalent impedance occurs at resonant frequency  $f_s$  not only depends on the quality factor  $Q$  but also depends on coupling coefficient  $k$ , which is a function of the geometrical dimension of two inductive coupling coils and their distances. Additionally, for an  $LC$  sensor with a sufficiently high-quality factor  $Q \gg 1$  and relatively small coupling coefficient  $k$  the equation (23) leads to a phase dip at

$$f_{\phi, \min} \approx \left(1 + \frac{1}{4}k^2\right) f_s \quad (24)$$

which is still a function of the coupling coefficient  $k$ . Hence, measuring the resonant frequency  $f_s$  of the sensor by utilising the phase dip approach requires a large  $Q$  to achieve a sharper dip in the impedance phase, and at the same time, it also requires keeping the  $k$  value smaller [62]. Phase dip



value can be calculated by the following expression [60]:

$$\Delta\varphi = \tan^{-1}(k^2Q) \quad (25)$$

Measurement of  $LC$  sensors in the phase dip technique requires a fixed distance and specific orientation between the sensor and reader coil in order to keep  $k$  not too large or not too low for accurately tracking the resonant frequency of the sensor. A larger value of  $k$  exhibits a wider phase dip, shifting the resonant frequency  $f_S$  to higher frequencies as shown in Fig. 5. (a), while a smaller value of  $k$  produces a smaller magnitude of the phase dip, which is harder to track and lowers the SNR of the sensor measurement. Moreover, measuring a sensor at a fixed wireless distance is not practical in many real-time wireless applications which often require sensor or reader movements. Aside from the optimal value of the coupling coefficient  $k$ , phase dip measurement necessitates a sensor with a high-quality factor  $Q$ , as illustrated in Fig. 5. (b). The higher the sensor  $Q$ , the larger and sharper the phase dip magnitude, and the better the SNR of the readout signal. A high  $Q$  factor  $LC$  sensor could be achieved by increasing the size of the inductive coil of the sensors while keeping the internal resistance of the inductive trace as low as possible which is always a tradeoff between them as expressed in equation (16).

## 2) DIP METER MEASUREMENT IN FREQUENCY DOMAIN

Instead of measuring the phase dip of the equivalent impedance, a more robust measurement technique has been reported by several research groups which measures the real part of the maximum equivalent impedance [63], [64]. Numerical simulation of the real part of equivalent impedance in equation (18), as shown in Fig. 5. (c), shows that the coupling coefficient  $k$  only acts as an amplitude scaling factor and is independent of the sensor's resonance frequency  $f_S$ , and quality factor  $Q$ . The maximum frequency  $f_{\max}$  and Full Width at Half Maximum (FWHM) can be obtained by following relations [59].

$$f_{\max} = \frac{2Q}{\sqrt{4Q^2 - 2}}f_S, \quad Q \approx \frac{f_S}{\Delta f_{\max}} \quad (26)$$

where  $f_{\max}$  is the maximum frequency which can be obtained from the maximum of  $R_e\{Z_1\}$  of equation (18), and  $\Delta f_{\max}$  is the FWHM of  $R_e\{Z_1\}$  at the origin of  $f_{\max}$ . Fig. 5. (d) shows the graphical representation of the  $\Delta f_{\max}$  for a sensor of  $Q$  value of 105. For sufficiently large quality factor  $Q \gg 1$ , the  $f_{\max}$  in equation (26) becomes the resonant frequency  $f_S$  of the sensor,  $f_{\max} \approx f_S$ , hence the sensor measurement is theoretically independent of the coupling coefficient  $k$ , and therefore distance independent measurement of the sensor. Moreover, one can obtain the value of the maximum impedance of the real part of equation (18) by setting  $f = f_S$  which can be expressed as [43]:

$$Z_{\max} = R_e(Z_1)_{\max}|_{f=f_S} = R_1 + 2\pi f_S L_1 k^2 Q \quad (27)$$

By comparing the effect of coupling coefficient  $k$  for both frequency domain measurement techniques, it is evident that the dip meter, or measuring the maximum real part of the equivalent impedance, provides theoretical distance-independent wireless measurement over the phase dip measurement technique as shown in Fig. 5. (c).

## B. TIME DOMAIN MEASUREMENT

In time domain or transient measurements, a pulse signal or modulated/ unmodulated signal is applied at the primary coil of the magnetic coupling for a short period of time, and damped decay response of the sensor is acquired at the primary or the readout coil of the sensor to determine the resonant frequency  $f_S$  and quality factor  $Q$  as shown in Fig. 6. (a) [39], [40]. The basic operating principle of the time domain measurement technique is depicted in Fig. 6. (b) and (c), respectively. In this measurement, sensor operation can be separated into two different phases of time: the excitation phase and the detection phase. The excitation phase provides an excitation signal to the sensors for a short period of time. The following time phase is called the detection phase which acquires the damped decay response of the sensors. Fischer et al. reported time domain measurement of a resonant sensor where the sensor's damped decay response  $f_d$  is measured at the secondary coil, which is an integral part of the sensor [27]. However, measuring the sensor response at the primary coil allows for complete isolation of the sensor from the reader, which is a more practical case for wireless resonant sensor measurement.

The analytical modeling of time domain measurement has considered sensors detection phase as shown in Fig. 6. (c), since the sensor excitation phase only provides the excitation signal to the sensor, which does not have an active role during the detection phase. The impedance of primary and secondary coils can be represented as  $Z_1 = R_1 + sL_1$  and  $Z_2 = R_2 + sL_2$ , respectively, where  $s$  is the complex frequency in the Laplace domain. During the detection phase, energy storage elements in an inductively coupled sensor circuit are no longer relaxed. For analytical analysis, one needs to consider the effects of initial conditions on the sensor readout signal, and for all the initial conditions  $t > 0$ , which only affects the starting amplitude of the readout signal and does not alter the complex frequency of the sensor [65]. Hence, the single initial condition denoted by  $V_{C20}$  can be considered an effective initial condition, which is the voltage across the capacitive sensor  $C_2$  at  $t = 0$ , neglecting other initial conditions as shown in Fig. 6. (d). The equivalent circuit for time domain measurement during the detection phase can be analysed in the Laplace domain and the readout signal can be expressed as follows [65]:

$$V_1(s) = k \sqrt{\frac{L_1}{L_2}} V_{C20} \frac{s}{s^2 + s \frac{R_2}{L_2} + \frac{1}{L_2 C_2}} \quad (28)$$

The corresponding expression of the readout signal  $V_1(s)$  can

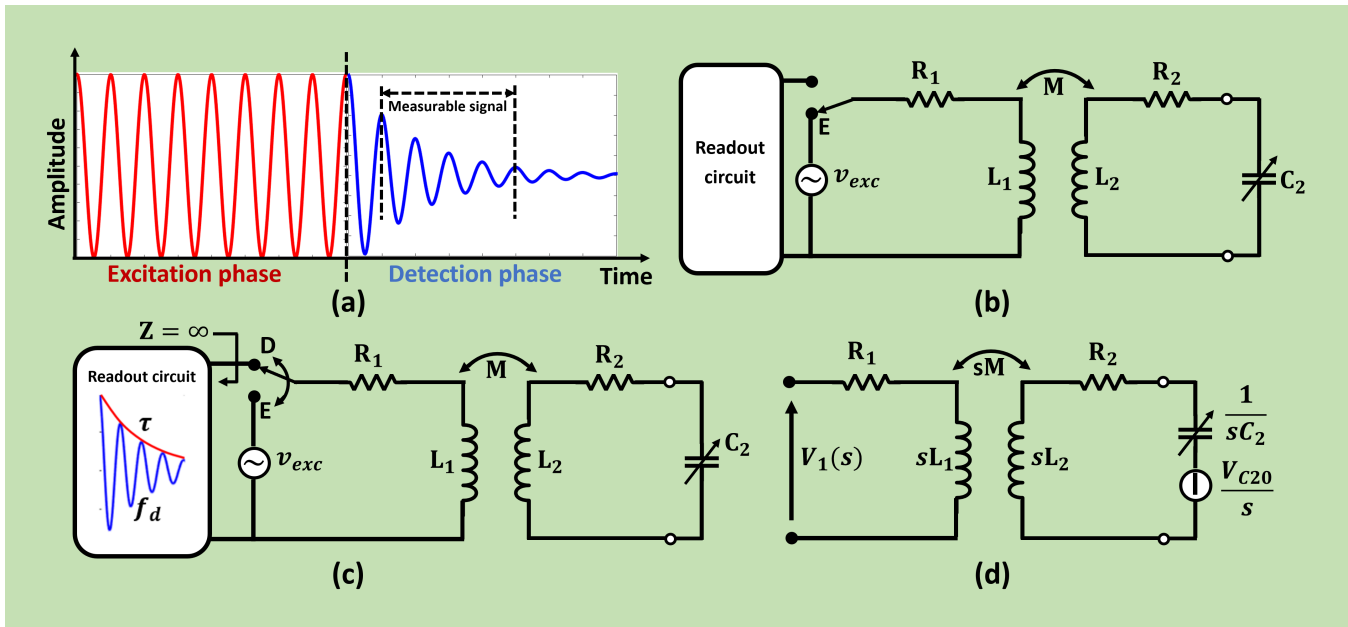


**FIGURE 6.** Block diagram of the time domain measurement technique, (a) excitation and detection signal representation of the time domain measurement, (b) block diagram of the excitation phase of the LC sensors [65], (c) block diagram of the detection phase of the LC sensors [65], (d) equivalent circuit of the LC sensors during the detection phase [65].

be calculated in the time domain

$$v_1(t) = kabV_{C20}e^{-\frac{t}{\tau_d}} \cos \left[ 2\pi f_d t - \tan^{-1} \left( \frac{1}{2\pi f_d \tau_d} \right) \right] \quad (29)$$

where  $a = \sqrt{\frac{L_1}{L_2}}$ , and  $b = \sqrt{\frac{4Q^2}{4Q^2-1}}$

The signal  $v_1(t)$  is a damped decay sinusoidal with a damped frequency  $f_d$  and decay time  $\tau_d$  which are connected to the resonant frequency  $f_s$  and quality factor  $Q$  of the sensor, and they can be expressed as follows:

$$f_d = \sqrt{1 + \frac{1}{4Q^2}} f_s, \quad \tau_d = \frac{Q}{\pi f_s} \quad (30)$$

where for a sufficiently larger  $Q$ , the damped frequency  $f_d$  becomes the resonant frequency  $f_s$  of the sensor as  $f_d \approx f_s$ , with a relative deviation  $|f_d - f_s|/f_s < 50$  for  $Q > 50$ . It can be observed from equation (29) that the coupling coefficient  $k$  only acts as an amplitude scaling factor of the damped sinusoidal signal  $v_1(t)$ , where the damped frequency  $f_d$  and decay time  $\tau_d$  are unaffected by coupling coefficient  $k$ . Therefore, the resonant frequency  $f_s$  of the wireless LC sensor in time domain measurement is theoretically independent of the coupling coefficient  $k$ . Fig. 7. (a) shows the readout signal  $v_1(t)$  for different values of  $k$ , which only affect the amplitude of the signal without altering the damped frequency  $f_d$ .

#### IV. MEASUREMENT CHALLENGES OF LC SENSORS

Analytical modeling of the wireless LC resonant sensors for two measurement techniques, dip meter in the frequency domain and transient or time domain measurement, showed that the resonant frequency  $f_s$  and quality factor  $Q$  of the sensor are theoretically independent of the coupling coefficient  $k$ ,

resulting in a distance-independent wireless measurement of the sensors. Nevertheless, when these two measurement techniques are utilised in real electronics equipment or circuits; unavoidable parasitic capacitance  $C_P$  appears in parallel to the readout coil, which comprises all the contributions from the parasitic capacitance present in the primary coil  $L_1$ , the capacitance of the connections, and the input capacitance of the electronic interface [65], [66]. The presence of finite parasitic capacitance  $C_P$  significantly degrades the measurement accuracy of the resonant frequency  $f_s$  and the quality factor  $Q$  of the sensors. The following sections discuss the effect of parasitic capacitance  $C_P$  for dip meter in frequency domain and time domain measurement as depicted in Fig. 8. (a) and Fig. 8. (b).

#### A. EFFECTS OF PARASITIC CAPACITANCE IN DIP METER MEASUREMENT

Limitations associated with measuring the maximum real part of the equivalent impedance in dip meter measurement in frequency domain are due to the presence of unavoidable finite parasitic capacitance  $C_P$ , which appears in parallel to the readout coil of the LC sensor as shown in Fig. 8. (a) [66]. When the presence of parasitic capacitance is not negligible, the real part of the equivalent impedance  $Z_{1P}$  becomes [66]:

$$R_e \{Z_{1P}\} = R_e \left\{ \frac{\left( m + \frac{4\pi^2 f^2 k^2 L_1 L_2}{R_2 + j2\pi f L_2 + \frac{1}{j2\pi f C_P}} \right) \frac{1}{j2\pi f C_P}}{m + \frac{4\pi^2 f^2 k^2 L_1 L_2}{R_2 + j2\pi f L_2 + \frac{1}{j2\pi f C_P}} + \frac{1}{j2\pi f C_P}} \right\} \quad (31)$$

where  $m = R_1 + j2\pi f L_1$ . Equation (31) shows that the coupling coefficient  $k$  not only acts as an amplitude scaling

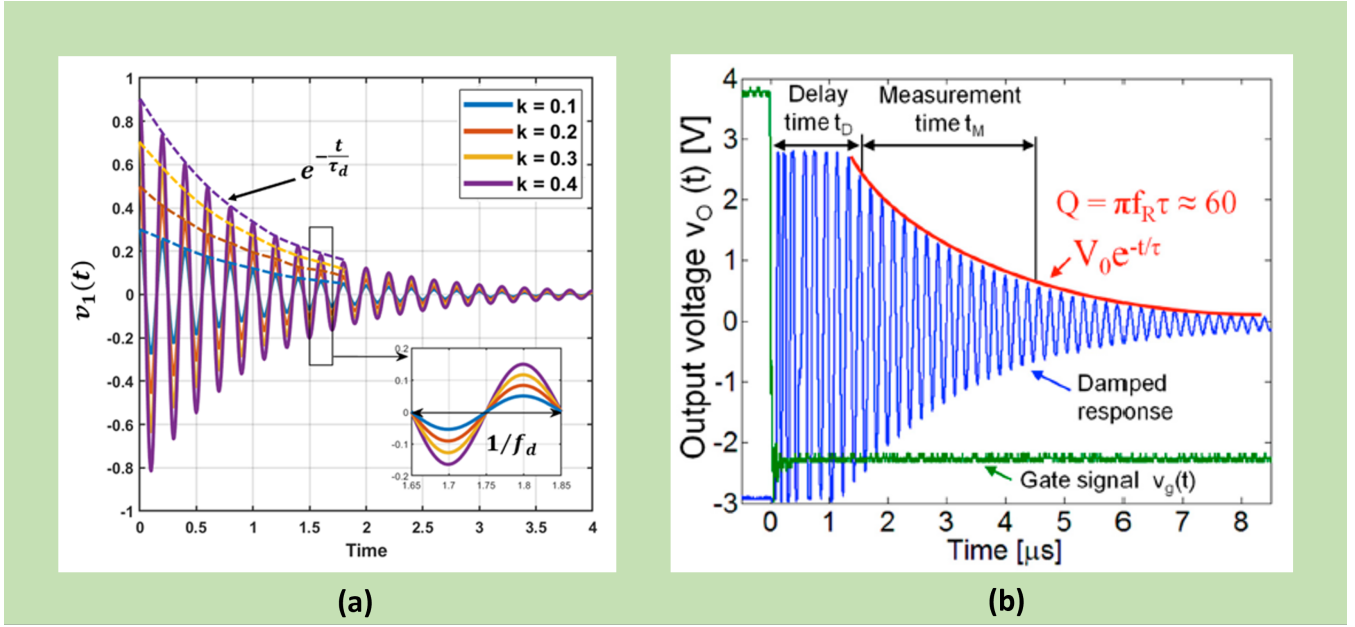


**FIGURE 7.** (a) Simulation on the effect of different values of coupling coefficient  $k$  on the amplitude and the length of the readout signal [65], (b) measured output voltage versus time during the detection phase of the sensors. The delay time  $t_D$  is used to avoid the initial glitch of the damped signal, and the measurement time  $t_M$  represents the sensor measurement time. The envelope of the damped decay signal approximates the quality factor of the sensor [39].

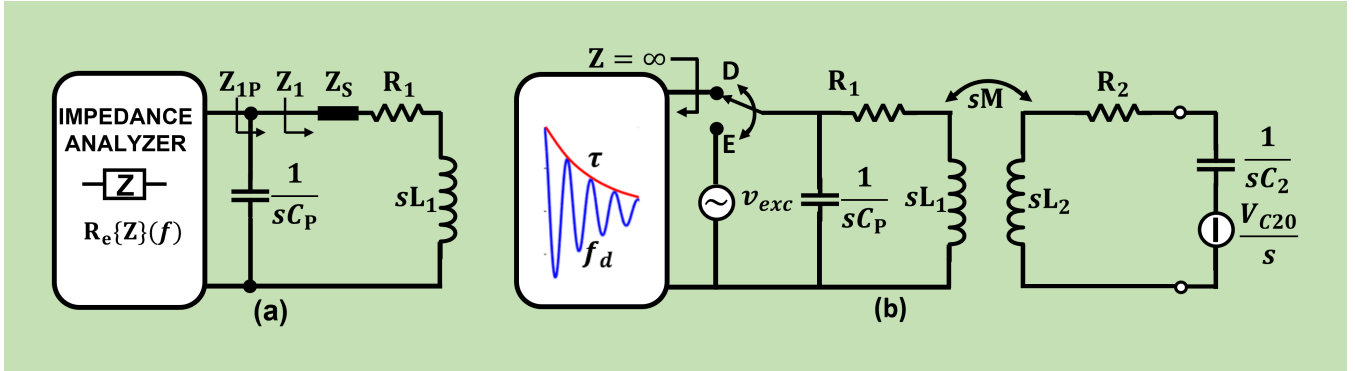


**FIGURE 8.** (a) Block diagram of the frequency domain measurement of wireless LC sensor by an impedance analyser with the presence of parasitic capacitance [65], (b) block diagram of the time domain measurement of the LC sensor and its equivalent circuit in Laplace domain under the presence of parasitic capacitance  $C_P$  in parallel to the readout signal [65].

factor but without knowing the value of  $k$  priori, it is not possible to extract the resonant frequency  $f_S$ , and quality factor  $Q$  of the sensor independently. The numerical analysis illustrates that there are two maxima of the real part of equivalent impedance  $Z_{1P}$  are influenced by the coupling coefficient  $k$ —when parasitic capacitance  $C_P$  is fixed and coupling coefficient  $k$  is variable in Fig. 9. (a); and parasitic capacitance  $C_P$  is variable while coupling coefficient  $k$  is fixed in Fig. 9. (b)—corresponds to a primary resonance near  $f_S = 1/(2\pi\sqrt{L_2C_2})$  and a secondary resonance near  $f_P = 1/(2\pi\sqrt{L_1C_P})$ , respectively [66], [67]. The numerical simulation and the measurement result exhibit that when  $C_P$  is non-negligible, the maximum real of the equivalent impedance is not distance independent as shown in Fig. 9. (a) and (b), and Fig. 10. (a) indicating no compensation,

respectively.

### B. EFFECTS OF PARASITIC CAPACITANCE IN TIME DOMAIN MEASUREMENT

The analytical modeling of time domain measurement discussed in section (III) B showed that the damped frequency  $f_d$  of the sensor is theoretically independent of the wireless interrogation distance. However, the analytical expression of time domain measurement by considering the parasitic capacitance was derived in the Laplace domain, and it could be written as [65]:

$$V_{1P}(s) = k\sqrt{\frac{L_1}{L_2}} \frac{sV_{C20}C_2L_2}{s^4C_2C_PL_1L_2(1-k^2) + s^3x + s^2y + s\zeta + 1} \quad (32)$$

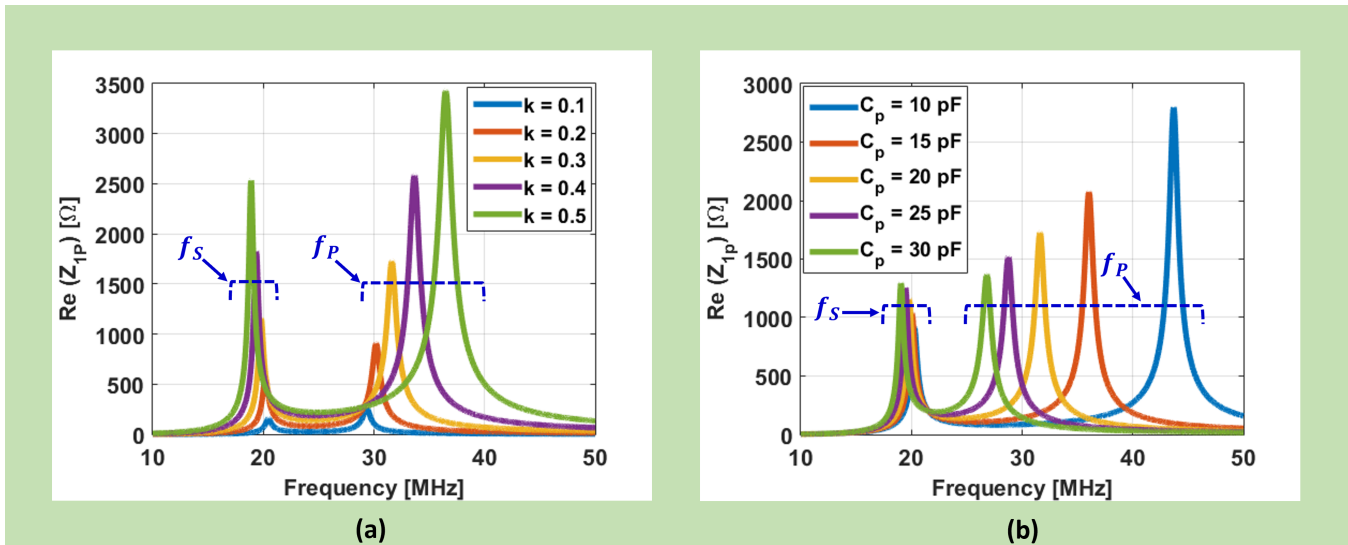


**FIGURE 9.** (a) Numerical simulation of the real part of equivalent impedance under the presence of parasitic capacitance  $C_p$  with increasing values of coupling coefficient  $k$  [67], (b) simulation of the real part with varying parasitic capacitance [67].

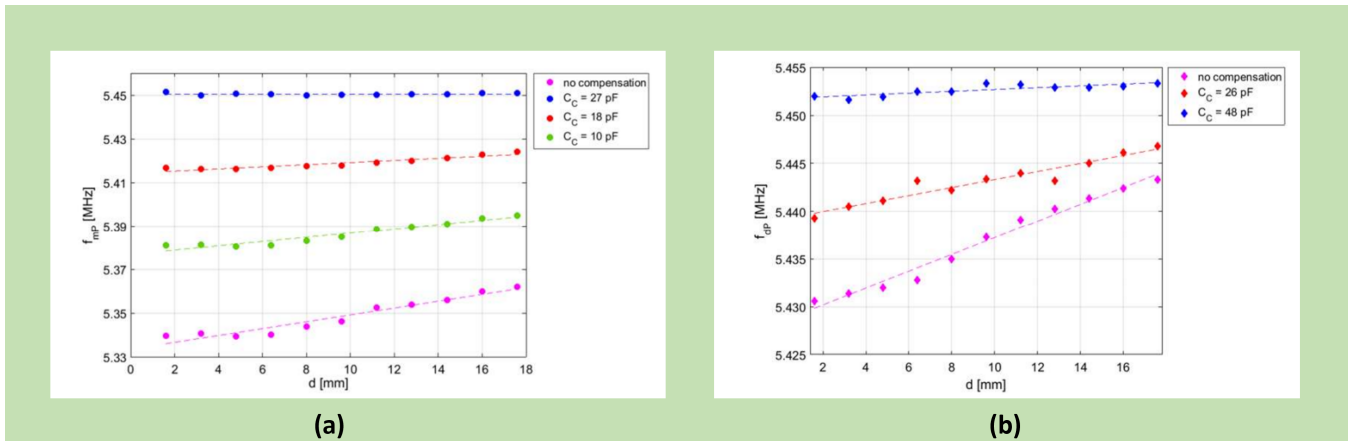


**FIGURE 10.** (a) Measurement of the maximum real part of  $Re\{Z_1\}$  for different wireless interrogation distance without using capacitance compensation circuit indicating as no compensation and with capacitance compensation circuit in parallel to the readout coil as indicated  $C_p$  [65], (b) measurement of the damped decay response for different wireless distances without capacitance compensation circuit indicating no compensation and with a capacitance compensation circuit indicating  $C_p$  [65].

where

$$\begin{aligned} x &= C_2 C_p (L_1 R_2 + L_2 R_1), \\ y &= C_2 L_2 + C_p L_1 + C_2 C_p R_1 R_2, \\ z &= C_2 R_2 + C_p R_1 \end{aligned}$$

It can be seen from equation (32) that the coupling coefficient  $k$  is not only acting as an amplitude scaling factor but is also connected to the coefficient of the fourth-order polynomial at the denominator. Since the fourth order polynomial can be decomposed into two pairs of complex conjugate roots and the  $S^4$  term is connected to the coupling coefficient in the form of  $(1 - k^2)$ , it is expected that the complex frequencies (for  $s = j\omega$ ) will depend on  $k$ . The inverse Laplace transform of the equation (32) shows that the output voltage signal composed of the sum of two damped sinusoids and can be

expressed as follows:

$$v_{1C_p}(t) = A_1 e^{-\frac{t}{\tau_{d1}}} \cos(\omega_{d1}t - \theta_1) + A_2 e^{-\frac{t}{\tau_{d2}}} \cos(\omega_{d2}t - \theta_2) \quad (33)$$

where  $A_1$  and  $A_2$  are the amplitude coefficients,  $\theta_1$  and  $\theta_2$  are the phase angle of the readout signal, which depends on the parameters of the circuits and the initial conditions. Damped frequencies  $\omega_{d1}$  and  $\omega_{d2}$ , and the decay times  $\tau_{d1}$  and  $\tau_{d2}$  can be obtained from two pairs of complex conjugate poles by setting the denominator of the equation (32) equal to zero. The values of the two pairs of complex conjugate poles can be further derived and seen that the decay time  $\tau_{d2}$  is larger than  $\tau_{d1}$  and, the resulting damped sinusoid  $\omega_{d1}$  falls faster than that  $\omega_{d2}$ . Since both  $\omega_{d1}$  and  $\omega_{d2}$  are dependent on the coupling coefficient  $k$ , the effect of parasitic capacitance  $C_p$  ceases the distance independent measurement

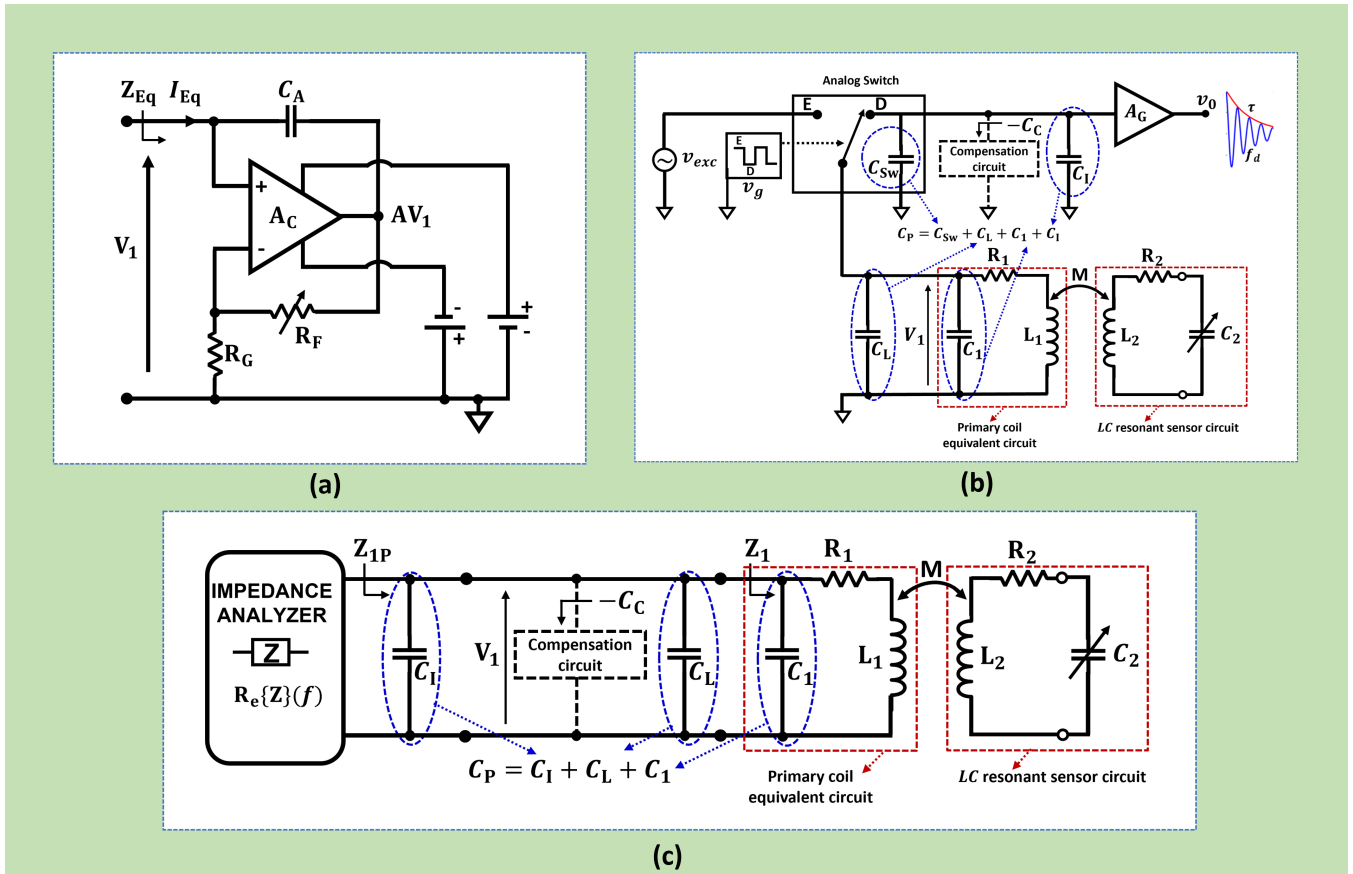


**FIGURE 11.** (a) Block diagram of the parasitic capacitance compensation circuit [67], (b) The effect of parasitic capacitance  $C_P$  appears in parallel to the readout coil of the LC sensor during the detection phase of the time domain measurement. The parasitic capacitance  $C_P$  is the sum of all the parasitic capacitance contributions such as capacitance of the analog switch  $C_{sw}$ , capacitance of the connection  $C_L$ , capacitance between traces of the primary coil  $C_1$ , and input capacitance of the readout amplifier  $C_i$  which appears in parallel to the readout coil. Parasitic capacitance compensation circuit is connected in parallel to the readout coil to cancel the effect of  $C_P$  [65], (c) the effect of  $C_P$  in frequency domain dip meter measurement. Different parasitic capacitance contributes to  $C_P$  in parallel to the readout coil namely impedance analyser input capacitance  $C_i$ , capacitance of the connection  $C_L$ , and capacitance between traces of primary coil  $C_1$ . A compensation circuit is employed in parallel to the readout coil to cancel the effect of  $C_P$  [65].

of the LC sensor. Therefore, the effect of parasitic capacitance is nonnegligible for distance-independent measurement of wireless LC sensors in both frequency and time domain, and the presence of parasitic capacitance  $C_P$  contributes to an inaccurate measurement of the resonant frequency  $f_S$ , and quality factor  $Q$  of the sensors.

## V. PARASITIC CAPACITANCE COMPENSATION TECHNIQUE

The presence of parasitic capacitance in parallel to the readout coil in both measurement techniques—dip meter in frequency domain and time domain—results in distance dependent measurement of the wireless LC resonant sensors. For dip meter measurement, the maximum real part of the equivalent impedance is theoretically independent of the distance, hence  $k$ , when parasitic capacitance  $C_P$  is not present in the readout coil as shown in numerical simulation in Fig. 5. (C). In contrast, when the parasitic capacitance  $C_P$  is non-negligible as shown in Fig. 11. (C), the maximum real part of equivalent impedance becomes distance dependent measurement of the

sensor, hence  $k$  dependent, as shown by numerical simulation in Fig. 9. (a), (b), and by the experimental result in Fig. 10. (a) indicating no compensation.

On the other hand, for time domain measurement, the damped decay response of the sensor is independent of the wireless distance and hence  $k$ , when the parasitic capacitance is not present at the readout coil as shown in numerical simulation Fig. 7. (a). However, the parasitic capacitance  $C_P$  appears during the detection phase of the sensor as shown in Fig. 11. (b). The experimental result shown in Fig. 10. (b) indicating no compensation validates the distance dependent measurement of the sensor when  $C_P$  is non-negligible.

Therefore, to overcome the effects of parasitic capacitance, a compensation circuit has been proposed by Demori et al. which can be connected to the sensor readout coil to eliminate the presence of unavoidable parasitic capacitance  $C_P$  for both frequency and time domain measurement and can significantly improve the accuracy of distance independent measurement of the sensors [65], [66]. The proposed circuit acts as a negative impedance converter which provides an

equivalent impedance, where negative capacitance can be tuned to compensate and possibly cancel the parasitic capacitance  $C_P$  [66], [67]. The Fig. 11. (a) shows the block diagram of the parasitic capacitance compensation circuit which is an operational amplifier with a positive feedback, and will be connected in parallel to the readout coil  $L_1$ . The induced voltage  $V_1$  across the readout coil  $L_1$  is then fed to the capacitance  $C_A$  and the current flowing through the capacitance  $C_A$  can be written as follows [66]:

$$I_1 = \frac{V_1 - AV_1}{\frac{1}{sC_A}} = -\frac{R_F}{R_G} sC_A V_1 \quad (34)$$

Where  $A = \left(1 + \frac{R_F}{R_G}\right)$  is the non-inverting gain of the operational amplifier. Therefore, the equivalent input impedance  $Z_{Eq}$  of the amplifier can be written from equation (34) as follows:

$$Z_{Eq} = \frac{V_1}{I_1} = -\frac{R_G}{R_F s C_A} = -\frac{R_G}{j\omega C_A R_F} = \frac{1}{j\omega (-C_c)} \quad (35)$$

Where  $-C_c = -C_A \frac{R_F}{R_G}$ , indicating that the circuit simulates an effective negative capacitance. From equation (35), if the gain of the amplifier is made adjustable, i.e. making the feedback resistor  $R_F$  as a variable resistance,  $-C_c$  can be tuned to compensate and possibly cancel the parasitic capacitance  $C_P$  [66], [67]. The cancellation of  $C_P$  will lead the equation (31) to become equation (18) as  $R_e \{Z_{1P}\} = R_e \{Z_1\}$  and equation (32) become in equation (28) as  $V_{1P}(S) = V_1(S)$ . Therefore, cancelation of the  $C_P$  results in distance independent measurement of  $LC$  resonant sensor in both measurement techniques: frequency domain in dip meter and time domain.

Fig. 10. (a) shows the measurement of the maximum real part of equivalent impedance for different wireless distances after introducing the parasitic compensation circuits as indicating  $C_C$  [65]. It can be observed that the resonant frequency  $f_S$  of the  $LC$  sensors which is the maximum real part of the equivalent impedance is identical throughout the variation of wireless interrogation distances when the compensation capacitance  $C_C=27$  pF, resulting in distance independent measurements. Similarly, the capacitance compensation circuit is employed to measure the damped frequency  $f_d$  of the  $LC$  sensors for different wireless distances in time domain measurement, as shown in Fig. 10. (b) indicating  $C_C$  [65]. It can be seen that without compensation circuit, the measurement of damped frequency  $f_d$  in time domain exhibits inaccuracies.

## VI. DISCUSSION

Wireless passive  $LC$  resonant sensors have been widely investigated in various fields of applications due to their numerous benefits. These benefit include passive operation, which eliminates the need for an active power supply. Their sensing elements, such as inductors and capacitors, are relatively easy to fabricate. These sensors have a robust sensing operating principle based on resonance and are suitable for handheld sensor applications. Despite all these advantages, the need

for complex or bulky readout systems remains a bottleneck for adoption of handheld wireless sensor measurements. For widespread application of  $LC$  sensors, it is of utmost importance to design a compact, simple, low power and cost-effective reader system, which is unavailable in current practice.

One of the most desirable features of the wireless  $LC$  sensor is to have an increased wireless interrogation distance. Since the  $LC$  sensor is formed with a combination of an inductive coil with a capacitor, increasing the size of the inductive coil can effectively increase the magnetic coupling between the sensor and readout coil, resulting in an increased wireless distance. However, increasing the size of the inductive coil that connects with the capacitive sensing element, increases the overall footprint of the  $LC$  sensor, which makes it difficult to deliver and place the sensor in many applications such as biomedical implantation. The advancement of micro-electromechanical systems (MEMS) and flexible printing technologies have enabled miniaturisation of sensor footprints but reducing the coil size of the sensor has a significant effect on the wireless interrogation distance and quality factor  $Q$  of the sensor, which essentially reduce the measurement distance and SNR of the readout signal.

In 2008, Chen et al., proposed parylene based micro-machined wireless  $LC$  pressure sensors with a footprint of  $4 \times 1$  mm<sup>2</sup>, an operating frequency of 150 MHz, and a quality factor of 5 that achieved the wireless distance of 2 mm [68]. Xue et al., developed an  $LC$  pressure sensors made of SU-8 and Gold with a footprint of  $3.23 \times 1.52 \times 0.2$  mm<sup>3</sup>, achieved a wireless distance of 6 mm, with operating frequency of 250 MHz, and a quality factor of 21.3 [69]. Later on Chen et al, developed an improved version of pressure sensor with parylene C having a quality factor of 30 which covers the wireless distance more than 20 mm with operating frequency of approximately 350 MHz, evidencing the increased wireless distance with improved quality factor  $Q$  of the sensor [70].

In order to increase the inductance value of the sensor coil, a multilayer inductor can be used as reported in [71], [72]. However, at high-frequency sensor operation, the parasitic capacitance between the inductive coil traces comes into play and needs careful handling. Moreover, the value of the inductive coil of the sensor can be increased by introducing a magnetic material such as a ferrite core with the inductive coil to obtain a stronger coupling between the wireless interrogating coils. Harpster et al. proposed a humidity sensor based on polyimide as sensitive capacitor and solenoid coil wound around a ferrite substrate to improve the wireless distance upto 20 mm [77]. However, integrating magnetic material further increases the size of the coil, and weight of the sensors.

A high-quality factor  $Q$  is always desirable for the wireless operation of the  $LC$  sensors which essentially increases the wireless interrogation distance between the sensor and reader and improves the accuracy of the sensor measurements.  $Q$  factor of the  $LC$  sensor can be improved by tackling the losses that are present in the sensors. These losses include copper conduction losses in inductive coil, dielectric losses in

**TABLE 1. Comparison of relative deviation of sensor operating frequency  $(f - f_s) / f_s$  across wireless distance ranges in different measurement techniques**

$L_2$	$C_2$	$R_2$	$f_s$	$Q$	Considered distance, d	$(f - f_s) / f_s$ (%)	Comments	Reference
3.5 $\mu$ H	5 pF	-	38 MHz	-	0-62 mm	4.71	Phase dip measurement technique in frequency domain, $(f - f_s) / f_s$ (%) derived from Fig. 8 in [73].	[73]
8.35 $\mu$ H	4.37 pF	9.35 $\Omega$	26.3 MHz	-	0-60 mm	10.8	Phase dip measurement technique in frequency domain, $(f - f_s) / f_s$ (%) derived from Fig. 4 in [74].	[74]
11.4 $\mu$ H	15 pF	-	12.2 MHz	-	0-6 mm	0.78	Gate dip measurement technique in frequency domain, $(f - f_s) / f_s$ (%) derived from Fig. 5 in [75].	[75]
1.92 $\mu$ H	0.397 pF	-	178 MHz	6.5	0-18 mm (vertical)	6.74	Phase dip measurement technique in frequency domain, $(f - f_s) / f_s$ (%) derived from Fig.8. (a) in [76]	[76]
1.92 $\mu$ H	0.397 pF	-	178 MHz	6.5	0-14 mm (horizontal)	7.86	Phase dip measurement technique in frequency domain, $(f - f_s) / f_s$ (%) derived from Fig.8. (a) in [76]	[76]
8.5 $\mu$ H	104.7 pF	3.2 $\Omega$	5.3 MHz	89	0-24 mm	0.02 <	Dip meter measurement technique in frequency domain with parasitic capacitance compensation circuit, $(f - f_s) / f_s$ (%) derived from Fig. 6 in [66]	[66]
8.51 $\mu$ H	100 pF	3.2 $\Omega$	5.45 MHz	91	1.6-17.6 mm	0.02 <	Dip meter measurement technique in frequency domain with parasitic capacitance compensation circuit, $(f - f_s) / f_s$ (%) derived from Fig. 19 in [65]	[65]
8.5 $\mu$ H	99 pF	3.2 $\Omega$	5.48 MHz	91.5	1.6-14.4 mm	0.02 <	Dip meter measurement technique in frequency domain with parasitic capacitance compensation circuit, $(f - f_s) / f_s$ (%) derived from Fig.4. (a) in [67]	[67]
8.51 $\mu$ H	100 pF	3.2 $\Omega$	5.45 MHz	91	1-17.6 mm	0.03 <	Time domain measurement with parasitic capacitance compensation circuit, $(f - f_s) / f_s$ (%) derived from Fig. 23 in [65]	[65]

dielectric material of the sensing element—capacitor—, skin effects, and radiation losses [78], [79]. The copper conduction losses are mainly the resistive loss which is always present for both low and high frequency sensor operation and can be compensated by selecting high conductive coil materials, resulting a lower equivalent series resistance of the coil. For high frequency applications, skin effects appear on coil surfaces which contributes to high frequency losses of the LC sensor. Such high frequency losses can be reduced by using litz wire to design inductive coil [80], [81]. The dielectric loss can be tackled by selecting low-loss dielectric material for the sensing element and the radiation loss can be tackled by shielding the sensor during high frequency operation.

Furthermore, it has been shown in section (III) that for both dip meter and phase dip sensor measurement, a high  $Q$  sensors provides a sharper peak in both measurements. The numerical simulation in Fig. 5. (d) shows that measuring the maximum of the real part of equivalent impedance for a sensor with a quality factor  $Q = 105$  is 2.3 times higher than measuring the maximum of the real part of equivalent impedance for a sensor with a  $Q = 25$ , resulting in a higher value of the equivalent impedance and, thus, an improved SNR for the readout signal. For time domain measurement, as reported in equation (30), the damped decay frequency becomes the

resonant frequency of the sensor when  $Q$  of the sensor is ensured. The damped decay signal for  $k = 0.4$  indicates the higher  $Q$  value than the  $k = 0.1$ , as shown in Fig. 7. (a), where the  $Q$  of the sensor is extracted from the exponential envelope of the decay signal as  $e^{-t/\tau_d}$ . Furthermore, Fig. 7. (a) shows that the amplitude and length of the decay signal increase with high  $Q$  value of the sensor. Therefore, measurability of the readout sensors greatly increases for high  $Q$  sensors for both frequency and time domain measurement, by improving the SNR of the readout signal.

The coupling coefficient  $k$  between the two inductive coils  $L_1$  and  $L_2$  has also a significant effect on the sensor readout signal, since  $k$  depends on the geometrical parameters of the coils such as their distances, and relative orientation. Hence, many wireless LC resonant sensor is measured by keeping such geometrical parameters fixed and constant. However, for practical wireless LC sensor operations, keeping the distance and alignment between the sensors coils fixed and constant is impractical and requires  $k$  independent measurement of the sensors. This review has shown that the measurement of the real part of the equivalent impedance of the readout coil in frequency domain, and measuring the voltage of the readout coil in the time domain are theoretically independent of the coupling coefficient  $k$ , hence not affected by the distance

between the sensor and the reader circuit. But the presence of parasitic capacitance, which appears in parallel with the readout coil of the sensor for both frequency and time domain measurement eliminates the integrity of  $k$  in a distance-independent wireless measurement of the sensors. To resolve the  $k$  dependence in these measurements, a compensation circuit is required to cancel the unavoidable parasitic capacitance. The Table 1 shows the comparison of relative deviation of the resonant frequency across wireless distance ranges in different measurement techniques with and without parasitic capacitance compensation circuit. It can be observed that the relative deviation of the resonant frequency significantly reduced to 0.02% for the measurement where a compensation circuit has been employed.

## VII. CONCLUSION

The fundamental operating principles of the wireless passive LC sensors, and their measurement techniques, such as time and frequency domain, have been reviewed, as well as how these two methods can precisely measure the resonance frequency of the sensor. Phase dip measurement in the frequency domain has been applied in many applications, but accurate sensor measurement using the phase dip technique requires a fixed wireless distance because phase dip measurement is highly dependent on the coupling coefficient  $k$ , and thus not suitable for wireless distance independent sensor measurement. The dip meter measurement in the frequency domain and the damped decay response in the time domain measurement, on the other hand, are theoretically independent of the  $k$ , resulting in distance independent wireless measurement of the sensor. However, both measurement techniques suffer from unavoidable parasitic capacitance which appears in parallel to the sensor's readout coil, resulting in a distance dependent wireless sensor measurement. Such undesired dependency due to the presence of parasitic capacitance can be reduced significantly or completely eliminated when a parasitic compensation circuit is employed in parallel to the readout coil. This information will be of great value for future development of LC sensors that require accurate wireless readout.

## REFERENCES

- [1] R. S. MACKAY and B. JACOBSON, "Endoradiosonde," *Nature*, vol. 179, no. 4572, pp. 1239–1240, Jun. 1957, 10.1038/1791239a0.
- [2] C. C. Collins, "Miniature Passive Pressure Transensor for Implanting in the Eye," *IEEE Transactions on Biomedical Engineering*, vol. BME-14, no. 2, pp. 74–83, 1967, 10.1109/TBME.1967.4502474.
- [3] S. E. Woodard, C. Wang and B.D. Taylor, "Wireless temperature sensing using temperature-sensitive dielectrics within responding electric fields of open-circuit sensors having no electrical connections." *Measurement Science and Technology*, vol. 21, no. 7, pp. 075201, May. 2010, 10.1088/0957-0233/21/7/075201.
- [4] C. Zhang, L. F. Wang, J. Q. Huang, and Q. A. Huang, "An LC-type passive wireless humidity sensor system with portable telemetry unit." *Journal of Microelectromechanical Systems*, vol. 24, no. 3, pp. 575–581, Jun. 2015, 10.1109/JMEMS.2014.2333747.
- [5] B. E. Horton, S. Schweitzer, A. J. DeRouin, and K.G. Ong, "A varactor-based, inductively coupled wireless pH sensor." *IEEE Sens J* vol. 11, no. 4, pp. 1061–1066, 2011, 10.1109/JSEN.2010.2062503.
- [6] S. H. Song, J. H. Park, G. Chitnis, R. A. Siegel, and B. Ziaie, "A wireless chemical sensor featuring iron oxide nanoparticle-embedded hydrogels," *Sens Actuators B Chem*, vol. 193, pp. 925–930, Mar. 2014, doi: 10.1016/J.SNB.2013.12.012.
- [7] M. Farooq et al., "Thin-Film Flexible Wireless Pressure Sensor for Continuous Pressure Monitoring in Medical Applications," *Sensors* 2020, Vol. 20, Page 6653, vol. 20, no. 22, p. 6653, Nov. 2020, doi: 10.3390/S20226653.
- [8] M. Farooq et al., "An Ex Vivo Study of Wireless Linkage Distance between Implantable LC Resonance Sensor and External Readout Coil," *Sensors* 2022, Vol. 22, Page 8402, vol. 22, no. 21, p. 8402, Nov. 2022, doi: 10.3390/S22218402.
- [9] M. Ferrari, M. Baù, M. Masud, and V. Ferrari, "A Time-gated Contactless Interrogation System for Frequency and Quality Factor Tracking in QCR to Investigate on Liquid Solution Microdroplets," *Procedia Eng*, vol. 168, pp. 704–707, Jan. 2016, doi: 10.1016/J.PROENG.2016.11.252.
- [10] M. Fonseca, M. Allen, J. Kroh, and J. White, "FLEXIBLE WIRELESS PASSIVE PRESSURE SENSORS FOR BIOMEDICAL APPLICATIONS," 2006.
- [11] C. M. Boutry, H. Chandrahali, P. Streit, M. Schinhammer, A. C. Hänzi, and C. Hierold, "Characterization of miniaturized RLC resonators made of biodegradable materials for wireless implant applications," *Sens Actuators A Phys*, vol. 189, pp. 344–355, Jan. 2013, doi: 10.1016/J.SNA.2012.08.039.
- [12] D. P. Rose et al., "Adhesive RFID sensor patch for monitoring of sweat electrolytes," *IEEE Trans Biomed Eng*, vol. 62, no. 6, pp. 1457–1465, Jun. 2015, doi: 10.1109/TBME.2014.2369991.
- [13] C. Girerd, Q. Zhang, A. Gupta, M. Dunna, D. Bharadia, and T. K. Morimoto, "Towards a Wireless Force Sensor Based on Wave Backscattering for Medical Applications," *IEEE Sens J*, vol. 21, no. 7, pp. 8903–8915, 2021, doi: 10.1109/JSEN.2021.3049225.
- [14] J. Philpott, J. Churm, V. Nasrollahi, S. Dimov, C. Anthony, and G. Cummins, "Wireless Measurement of the Degradation Rates of Thin Film Bioresorbable Metals Using Reflected Impedance," *IEEE Transactions on Semiconductor Manufacturing*, vol. 36, no. 1, pp. 14–21, 2023, doi: 10.1109/TSM.2022.3221267.
- [15] F. A. A. del C. Manzanos, R. R. Hughes, and A. J. Croxford, "Passive Wireless Mechanical Overload Sensing: Proof of Concept Using Agarose Hydrogels," *IEEE Trans Instrum Meas*, vol. 72, pp. 1–9, 2023, doi: 10.1109/TIM.2023.3291741.
- [16] W.-J. Deng, L.-F. Wang, L. Dong, and Q.-A. Huang, "Symmetric LC Circuit Configurations for Passive Wireless Multifunctional Sensors," *Journal of Microelectromechanical Systems*, vol. 28, no. 3, pp. 344–350, 2019, doi: 10.1109/JMEMS.2019.2901818.
- [17] Q. Tan, F. Lu, Y. Ji, H. Wang, W. Zhang, and J. Xiong, "LC temperature-pressure sensor based on HTCC with temperature compensation algorithm for extreme applications," *Sens Actuators A Phys*, vol. 280, pp. 437–446, 2018, doi: 10.1016/J.SNA.2018.08.021.
- [18] D. Lu et al., "Bioresorbable Wireless Sensors as Temporary Implants for In Vivo Measurements of Pressure," *Adv Funct Mater*, vol. 30, no. 40, Oct. 2020, doi: 10.1002/ADFM.202003754.
- [19] W.-J. Deng, L.-F. Wang, L. Dong, and Q.-A. Huang, "Symmetric LC Circuit Configurations for Passive Wireless Multifunctional Sensors," *Journal of Microelectromechanical Systems*, vol. 28, no. 3, pp. 344–350, 2019, doi: 10.1109/JMEMS.2019.2901818.
- [20] W. Gao et al., "Fully integrated wearable sensor arrays for multiplexed in situ perspiration analysis," *Nature*, vol. 529, no. 7587, pp. 509–514, 2016, doi: 10.1038/nature16521.
- [21] H. Dinis and P. M. Mendes, "A comprehensive review of powering methods used in state-of-the-art miniaturized implantable electronic devices," *Biosens Bioelectron*, vol. 172, p. 112781, 2021, doi: https://doi.org/10.1016/j.bios.2020.112781.
- [22] M. J. Bathaei et al., "Photolithography-Based Microfabrication of Biodegradable Flexible and Stretchable Sensors," *Advanced Materials*, vol. 35, no. 6, p. 2207081, Feb. 2023, doi: https://doi.org/10.1002/adma.202207081.
- [23] F. Springer, R. W. Günther, and T. Schmitz-Rode, "Aneurysm Sac Pressure Measurement with Minimally Invasive Implantable Pressure Sensors: An Alternative to Current Surveillance Regimes after EVAR?," *Cardiovasc Intervent Radiol*, vol. 31, no. 3, pp. 460–467, 2008, doi: 10.1007/s00270-007-9245-9.
- [24] Y. Honjol et al., "Current view and prospect: Implantable pressure sensors for health and surgical care," *Med Devices Sens*, vol. 3, no. 3, p. e10068, Jun. 2020, doi: https://doi.org/10.1002/mds3.10068.



- [25] W. Mullens, F. Sharif, M. Dupont, A. M. K. Rothman, and W. Wijns, "Digital health care solution for proactive heart failure management with the Cordella Heart Failure System: results of the SIRONA first-in-human study," *Eur J Heart Fail*, vol. 22, no. 10, pp. 1912–1919, Oct. 2020, doi: <https://doi.org/10.1002/ejhf.1870>.
- [26] A. I. Nunez and H. D. Rowland, "Wireless pressure sensor and method for fabricating wireless pressure sensor for integration with an implantable device," *US 7,677,107 B2*, Mar. 16, 2010.
- [27] W. J. Fischer et al., "Galfenol resonant sensor for indirect wireless osteosynthesis plate bending measurements," *Proceedings of IEEE Sensors*, pp. 611–616, 2009, doi: 10.1109/ICSENS.2009.5398320.
- [28] L. Lin, M. Ma, F. Zhang, F. Liu, Z. Liu, and Y. Li, "Integrated passive wireless pressure and temperature dual-parameter sensor based on LTCC technology," *Ceram Int*, vol. 44, pp. S129–S132, 2018, doi: <https://doi.org/10.1016/j.ceramint.2018.08.159>.
- [29] S. Charkhabi, K. J. Jackson, A. M. Beierle, A. R. Carr, E. M. Zellner, and N. F. Reuel, "Monitoring Wound Health through Bandages with Passive LC Resonant Sensors," *ACS Sens*, vol. 6, no. 1, pp. 111–122, Jan. 2021, doi: 10.1021/ACSSENSORS.0C01912/ASSET/IMAGES/LARGE/SE0C019120010.JPG.
- [30] P. Yeon, M. Kim, O. Brand, and M. Ghoovanloo, "Optimal Design of Passive Resonating Wireless Sensors for Wearable and Implantable Devices," *IEEE Sens J*, vol. 19, no. 17, pp. 7460–7470, 2019, doi: 10.1109/JSEN.2019.2915299.
- [31] H. Wen et al., "Array Integration and Far-Field Detection of Biocompatible Wireless LC Pressure Sensors," *Small Methods*, vol. 5, no. 3, p. 2001055, Mar. 2021, doi: 10.1002/SMTD.202001055.
- [32] M. A. Carvajal, P. Escobedo, A. Martínez-Olmos, and A. J. Palma, "Readout Circuit With Improved Sensitivity for Contactless LC Sensing Tags," *IEEE Sens J*, vol. 20, no. 2, pp. 885–891, 2020, doi: 10.1109/JSEN.2019.2943002.
- [33] G. Qin, L. Yang, Z. Fan, H. Dong, and S. Yu, "Optimization and design of bending-insensitive paper-based LC wireless passive sensors," *Microw Opt Technol Lett*, vol. 63, no. 11, pp. 2763–2768, Nov. 2021, doi: <https://doi.org/10.1002/mop.32968>.
- [34] Y. C. Lin, M. X. Cai, and Y. J. Yang, "A wireless passive pressure sensor using microstructured ferromagnetic films with tunable effective permeability," *Journal of Micromechanics and Microengineering*, vol. 31, no. 4, p. 045017, Mar. 2021, doi: 10.1088/1361-6439/ABEA04.
- [35] J. Garcia-Canton, A. Merlos, and A. Baldi, "High-quality factor electrolyte insulator silicon capacitor for wireless chemical sensing," *IEEE Electron Device Letters*, vol. 28, no. 1, pp. 27–29, Jan. 2007, doi: 10.1109/LED.2006.888189.
- [36] B. Lin, Q. Tan, G. Zhang, L. Zhang, Y. Wang, and J. Xiong, "Temperature and Pressure Composite Measurement System Based on Wireless Passive LC Sensor," *IEEE Trans Instrum Meas*, vol. 70, 2021, doi: 10.1109/TIM.2020.3031157.
- [37] R. Nopper, R. Has, and L. Reindl, "A wireless sensor readout system-circuit concept, simulation, and accuracy," *IEEE Trans Instrum Meas*, vol. 60, no. 8, pp. 2976–2983, Aug. 2011, doi: 10.1109/TIM.2011.2122110.
- [38] C. Zhang, S.-Y. Zhang, and L.-F. Wang, "A Sawtooth MEMS Capacitive Strain Sensor for Passive Telemetry in Bearings," *IEEE Sens J*, vol. 21, no. 20, pp. 22527–22535, 2021, doi: 10.1109/JSEN.2021.3107441.
- [39] M. Masud, M. Baù, M. Demori, M. Ferrari, and V. Ferrari, "Contactless Interrogation System for Capacitive Sensors with Time-Gated Technique," *Proceedings 2017*, Vol. 1, Page 395, vol. 1, no. 4, p. 395, Aug. 2017, doi: 10.3390/PROCEEDINGS1040395.
- [40] M. Demori, M. Masud, M. Bau, M. Ferrari, and V. Ferrari, "Passive LC sensor label with distance-independent contactless interrogation," *Proceedings of IEEE Sensors*, vol. 2017-December, pp. 1–3, Dec. 2017, doi: 10.1109/ICSENS.2017.8234410.
- [41] C. Li et al., "Review of Research Status and Development Trends of Wireless Passive LC Resonant Sensors for Harsh Environments," *Sensors (Basel)*, vol. 15, no. 6, pp. 13097–13109, Jun. 2015, doi: 10.3390/S150613097.
- [42] I. Bhar and N. Mandal, "A review on advanced wireless passive temperature sensors," *Measurement*, vol. 187, p. 110255, 2022, doi: <https://doi.org/10.1016/j.measurement.2021.110255>.
- [43] Q. A. Huang, L. Dong, and L. F. Wang, "LC Passive Wireless Sensors Toward a Wireless Sensing Platform: Status, Prospects, and Challenges," *Journal of Microelectromechanical Systems*, vol. 25, no. 5, pp. 822–841, Oct. 2016, doi: 10.1109/JMEMS.2016.2602298.
- [44] M. H. M. Kouhani, J. Wu, A. Tavakoli, A. J. Weber, and W. Li, "Wireless, passive strain sensor in a doughnut-shaped contact lens for continuous non-invasive self-monitoring of intraocular pressure," *Lab Chip*, vol. 20, no. 2, pp. 332–342, 2020, doi: 10.1039/C9LC00735K.
- [45] M. H. M. Kouhani, A. Weber, and W. Li, "Wireless intraocular pressure sensor using stretchable variable inductor," *Proceedings of the IEEE International Conference on Micro Electro Mechanical Systems (MEMS)*, pp. 557–560, Feb. 2017, doi: 10.1109/MEMSYS.2017.7863467.
- [46] G. Z. Chen, I. S. Chan, L. K. K. Leung, and D. C. C. Lam, "Soft wearable contact lens sensor for continuous intraocular pressure monitoring," *Med Eng Phys*, vol. 36, no. 9, pp. 1134–1139, Sep. 2014, doi: 10.1016/J.MEDENGGPHY.2014.06.005.
- [47] F. Solitro et al., "Planar Elliptical Inductor Design for Wireless Implantable Medical Devices," *Bioengineering 2023*, Vol. 10, Page 151, vol. 10, no. 2, p. 151, Jan. 2023, doi: 10.3390/BIOENGINEERING10020151.
- [48] H. A. Wheeler, "Simple Inductance Formulas for Radio Coils," *Proceedings of the Institute of Radio Engineers*, vol. 16, no. 10, pp. 1398–1400, 1928, doi: 10.1109/JRPROC.1928.221309.
- [49] S. S. Mohan, M. D. M. Hershenson, S. P. Boyd, and T. H. Lee, "Simple accurate expressions for planar spiral inductances," *IEEE J Solid-State Circuits*, vol. 34, no. 10, pp. 1419–1420, 1999, doi: 10.1109/4.792620.
- [50] Z. Ma, Y. Zhang, K. Zhang, H. Deng, and Q. Fu, "Recent progress in flexible capacitive sensors: Structures and properties," *Nano Materials Science*, 2022, doi: <https://doi.org/10.1016/j.nanoms.2021.11.002>.
- [51] R. B. Mishra, N. El-Atab, A. M. Hussain, and M. M. Hussain, "Recent Progress on Flexible Capacitive Pressure Sensors: From Design and Materials to Applications," *Adv Mater Technol*, vol. 6, no. 4, p. 2001023, Apr. 2021, doi: <https://doi.org/10.1002/admt.202001023>.
- [52] G. Z. Chen, I. S. Chan, and D. C. C. Lam, "Capacitive contact lens sensor for continuous non-invasive intraocular pressure monitoring," *Sens Actuators A Phys*, vol. 203, pp. 112–118, Dec. 2013, doi: 10.1016/J.SNA.2013.08.029.
- [53] P. J. Chen, S. Saati, R. Varma, M. S. Humayun, and Y. C. Tai, "Wireless intraocular pressure sensing using microfabricated minimally invasive flexible-coiled LC sensor implant," *Journal of Microelectromechanical Systems*, vol. 19, no. 4, pp. 721–734, Aug. 2010, doi: 10.1109/JMEMS.2010.2049825.
- [54] W. Olthuis, W. Streekstra, and P. Bergveld, "Theoretical and experimental determination of cell constants of planar-interdigitated electrolyte conductivity sensors," *Sens Actuators B Chem*, vol. 24, no. 1–3, pp. 252–256, Mar. 1995, doi: 10.1016/0925-4005(95)85053-8.
- [55] J. Bird, *Bird's Electrical Circuit Theory and Technology, Second*. London: Routledge, 2021. doi: 10.1201/9781003130338.
- [56] M. Baù, M. Ferrari, and V. Ferrari, "Analysis and Validation of Contactless Time-Gated Interrogation Technique for Quartz Resonator Sensors," *Sensors 2017*, Vol. 17, Page 1264, vol. 17, no. 6, p. 1264, Jun. 2017, doi: 10.3390/S17061264.
- [57] "Communicating with implanted wireless sensor - Patent US-7245117-B1 - PubChem." <https://pubchem.ncbi.nlm.nih.gov/patent/US-7245117-B1> (accessed Jun. 23, 2023).
- [58] J. T. Farrar, C. Berkley, and V. K. Zworykin, "Telemetry of intraenteric pressure in man by an externally energized wireless capsule," *Science*, vol. 131, no. 3416, p. 1814, 1960, doi: 10.1126/SCIENCE.131.3416.1814.
- [59] R. Nopper, R. Niekrawietz, and L. Reindl, "Wireless readout of passive LC sensors," *IEEE Trans Instrum Meas*, vol. 59, no. 9, pp. 2450–2457, Sep. 2010, doi: 10.1109/TIM.2009.2032966.
- [60] A. Baldi, W. Choi, and B. Ziaie, "A self-resonant frequency-modulated micromachined passive pressure transducer," *IEEE Sens J*, vol. 3, no. 6, pp. 728–733, Dec. 2003, doi: 10.1109/JSEN.2003.820362.
- [61] A. DeHennis and K. D. Wise, "A double-sided single-chip wireless pressure sensor," *Proceedings of the IEEE Micro Electro Mechanical Systems (MEMS)*, pp. 252–255, 2002, doi: 10.1109/MEMSYS.2002.984250.
- [62] T. J. Harpster, B. Stark, and K. Najafi, "A passive wireless integrated humidity sensor," *Proceedings of the IEEE Micro Electro Mechanical Systems (MEMS)*, pp. 553–557, 2001, doi: 10.1109/MEMSYS.2001.906601.
- [63] S. L. Martínez, R. Giannetti, and J. L. R. Marrero, "Design of a system for continuous Intraocular Pressure monitoring," *Conference Record - IEEE Instrumentation and Measurement Technology Conference*, vol. 3, pp. 1693–1696, 2004, doi: 10.1109/IMTC.2004.1351407.
- [64] A. Babu and B. George, "A linear and high sensitive interfacing scheme for wireless passive LC sensors," *IEEE Sens J*, vol. 16, no. 23, pp. 8608–8616, Dec. 2016, doi: 10.1109/JSEN.2016.2614816.
- [65] M. Demori, M. Baù, M. Ferrari, and V. Ferrari, "Interrogation Techniques and Interface Circuits for Coil-Coupled Passive Sensors," *Micromachines (Basel)*, vol. 9, no. 9, 2018, doi: 10.3390/MI9090449.

- [66] M. Demori, M. Baù, M. Ferrari, and V. Ferrari, "Electronic technique and circuit topology for accurate distance-independent contactless readout of passive LC sensors," *AEU - International Journal of Electronics and Communications*, vol. 92, pp. 82–85, Aug. 2018, doi: 10.1016/j.aeue.2018.05.019.
- [67] M. Baù, M. Demori, M. Ferrari, and V. Ferrari, "Contactless Readout of Passive LC Sensors with Compensation Circuit for Distance-Independent Measurements," *Proceedings 2018*, Vol. 2, Page 842, vol. 2, no. 13, p. 842, Dec. 2018, doi: 10.3390/PROCEEDINGS2130842.
- [68] P. J. Chen, D. C. Rodger, S. Saati, M. S. Humayun, and Y. C. Tai, "Microfabricated implantable parylene-based wireless passive intraocular pressure sensors," *Journal of Microelectromechanical Systems*, vol. 17, no. 6, pp. 1342–1351, 2008, doi: 10.1109/JMEMS.2008.2004945.
- [69] N. Xue, S.-P. Chang, and J.-B. Lee, "A SU-8-Based Microfabricated Implantable Inductively Coupled Passive RF Wireless Intraocular Pressure Sensor," *Journal of Microelectromechanical Systems*, vol. 21, no. 6, pp. 1338–1346, 2012, doi: 10.1109/JMEMS.2012.2206072.
- [70] P. J. Chen, S. Saati, R. Varma, M. S. Humayun, and Y. C. Tai, "Wireless intraocular pressure sensing using microfabricated minimally invasive flexible-coiled LC sensor implant," *Journal of Microelectromechanical Systems*, vol. 19, no. 4, pp. 721–734, Aug. 2010, doi: 10.1109/JMEMS.2010.2049825.
- [71] A. DeHennis and K. D. Wise, "A double-sided single-chip wireless pressure sensor," *Proceedings of the IEEE Micro Electro Mechanical Systems (MEMS)*, pp. 252–255, 2002, doi: 10.1109/MEMSYS.2002.984250.
- [72] T. J. Harpster, B. Stark, and K. Najafi, "A passive wireless integrated humidity sensor," *Proceedings of the IEEE Micro Electro Mechanical Systems (MEMS)*, pp. 553–557, 2001, doi: 10.1109/MEMSYS.2001.906601.
- [73] M. Nowak, N. Delorme, F. Conseil, and G. Jacquemod, "Sensitivity analysis of a passive inductive telemetry system for a capacitive sensor," in *2006 Ph.D. Research in Microelectronics and Electronics*, 2006, pp. 273–276, doi: 10.1109/RME.2006.1689949.
- [74] C. Li, Q.-L. Tan, C.-Y. Xue, W.-D. Zhang, Y.-Z. Li, and J.-J. Xiong, "Wireless contactless pressure measurement of an LC passive pressure sensor with a novel antenna for high-temperature applications\*," *Chinese Physics B*, vol. 24, no. 4, p. 048801, 2015, doi: 10.1088/1674-1056/24/4/048801.
- [75] J. C. Butler, A. J. Vigliotti, F. W. Verdi, and S. M. Walsh, "Wireless, passive, resonant-circuit, inductively coupled, inductive strain sensor," *Sens Actuators A Phys*, vol. 102, no. 1, pp. 61–66, 2002, doi: [https://doi.org/10.1016/S0924-4247\(02\)00342-4](https://doi.org/10.1016/S0924-4247(02)00342-4).
- [76] M.-Z. Xie, L.-F. Wang, L. Dong, W.-J. Deng, and Q.-A. Huang, "Low Cost Paper-Based LC Wireless Humidity Sensors and Distance-Insensitive Readout System," *IEEE Sens J*, vol. 19, no. 12, pp. 4717–4725, 2019, doi: 10.1109/JSEN.2019.2901004.
- [77] T. J. Harpster, S. Hauvespre, M. R. Dokmeci, and K. Najafi, "A passive humidity monitoring system for in situ remote wireless testing of micropackages," *Journal of Microelectromechanical Systems*, vol. 11, no. 1, pp. 61–67, Feb. 2002, doi: 10.1109/84.982864.
- [78] M. Schormans, V. Valente, and A. Demosthenous, "Practical Inductive Link Design for Biomedical Wireless Power Transfer: A Tutorial," *IEEE Trans Biomed Circuits Syst*, vol. 12, no. 5, pp. 1112–1130, 2018, doi: 10.1109/TBCAS.2018.2846020.
- [79] Islam Asraf B, Islam Syed K, and Tulip Fahmida S, "Design and Optimization of Printed Circuit Board Inductors for Wireless Power Transfer System," *Circuits and Systems*, vol. 4, no. 2, pp. 237–244, Apr. 2013.
- [80] A. Ammouri, T. Ben Salah, and H. Morel, "A spiral planar inductor: An experimentally verified physically based model for frequency and time domains," *International Journal of Numerical Modelling: Electronic Networks, Devices and Fields*, vol. 31, no. 1, p. e2272, Jan. 2018, doi: <https://doi.org/10.1002/jnm.2272>.
- [81] W. B. Kuhn and N. M. Ibrahim, "Analysis of current crowding effects in multilayer spiral inductors," *IEEE Trans Microw Theory Tech*, vol. 49, no. 1, pp. 31–38, 2001, doi: 10.1109/22.899959.
- [82] M. Farooq, B. Amin, A. Elahi, W. Wijns, and A. Shahzad, "Planar Elliptical Inductor Design for Wireless Implantable Medical Devices," *Bioengineering*, vol. 10, no. 2, 2023, doi: 10.3390/bioengineering10020151.



**MEHEDI. MASUD** received the B.S. degree in Electrical and Electronic Engineering from Bangladesh, and M.S. degree in Electronics Engineering from the Politecnico di Milano, and the Ph.D. degree in Information Engineering major in Electronics Engineering, Sensors and Instrumentation from the University of Brescia, Italy, in 2018. His Ph.D. research was focused on the development of proximity contactless interrogation system for passive resonant sensors such as Quartz Crystal Microbalance, and Capacitive sensors. From 2019 to 2021, he was a postdoctoral researcher at Shanghai Jiao Tong University, China. His research interests include signal conditioning circuits for sensors, wireless implantable sensors, and sensor's application in therapeutic drug monitoring. He has been a postdoctoral researcher in Smart Sensors Laboratory, at University of Galway, Ireland, since 2022. He collaborates with the startup company SymPhysis MEDICAL on an industrial project to develop pressure sensors for medical devices.



**PATRICIA. VAZQUEZ** is a postdoctoral researcher with a background in MEMS sensors for biomedical problems. She obtained her PhD at DTU Nanotech in micro-technology. She has applied her expertise in a wide variety of MEMS sensors for applications such as environmental pollution and medical devices. In recent years she has focused on devices for cardiovascular pressure monitoring. Her current interests are cardiac implants and their deployment, in addition to point of care solutions that contribute to safer monitoring and treatment of patients from their homes.



**MUHAMMAD RIAZ UR REHMAN. REHMAN** (Graduate Student Member, IEEE) received a B.S. degree in computer engineering and an M.S. degree in electrical engineering from the University of Engineering and Technology, Taxila, Pakistan, in 2007 and 2011, respectively. He received a Ph.D. degree in electronics and electrical engineering from Sungkyunkwan University, Suwon, South Korea in 2020. His research interests include the implementation of analog/digital mixed-mode VLSI system design, Biomedical sensors, CMOS RF transceivers, and analog integrated circuits.



**ADNAN. ELAHI** is a lecturer in Medical Electronics and Co-director of the Translational Medical Device Lab at the University of Galway. He holds a PhD in Electronic Engineering and M.Sc. in Data Analytics from the University of Galway, an M.Sc. in Embedded Digital Systems from the University of Sussex, United Kingdom and a BS in Computer Engineering from COMSATS University, Pakistan. His PhD research was focused on the investigation and development of novel signal processing algorithms to improve microwave imaging of the breast. His current research spans the disciplines of engineering and medicine, with a particular focus on smart devices for remote patient monitoring; novel and personalised therapeutics using RF/Microwave and Pulsed-Field Ablation; and AI/machine learning for biomedical signals.



**WILLIAM. WIJNS** received the M.D. degree in cardiology and the Ph.D. degree from the University of Louvain Medical School, Belgium. After working at Erasmus University, The Netherlands, UCLA, University of Louvain, and the Cardiovascular Research Center Aalst, he joined the National University of Ireland Galway as a Science Foundation Ireland Research Professor Awardee, in 2016, and co-directing the Smart Sensors Laboratory, University of Galway. His research focuses

on the development and evaluation of novel device-based therapies for cardiovascular diseases. Ongoing projects aim to prevent high-risk subjects from suffering cardiac disability by modification of vulnerable plaques and modulation of trigger mechanisms that precipitate acute events. Dr. Wijns is currently the Chairman of PCR, an educational platform that connects the interventional cardiology community across the globe.



**ATIF. SHAHZAD** received the B.S. degree in computer engineering from COMSATS University, Lahore, Pakistan, in 2006, the M.S. degree in electronic and electrical engineering from the University of Leeds, U.K., in 2009, and the Ph.D. degree in electrical engineering from the University of Galway, Ireland, in 2017. He is an Honorary Lecturer with the School of Medicine, University of Galway, and a Research Fellow with the Institute of Metabolism and Systems Research, University

of Birmingham. He is also the Joint Director of the Smart Sensors Laboratory, School of Medicine, NUI Galway. His research interests include biosensing and medical technologies, medical signal and image processing, applied electromagnetics, and computational modeling. He is also a Topic Editor of BIOSENSORS journal.

...